

Three-Body Scattering at Intermediate Energies

H. Liu, Ch. Elster

*Institute of Nuclear and Particle Physics,
and Department of Physics and Astronomy,
Ohio University, Athens, OH 45701*

W. Glöckle

Institute for Theoretical Physics II, Ruhr-University Bochum, D-44780 Bochum, Germany.

(Dated: May 23, 2019)

The Faddeev equation for three-body scattering at arbitrary energies is formulated in momentum space and directly solved in terms of momentum vectors without employing a partial wave decomposition. In its simplest form the Faddeev equation for identical bosons, which we are using, is a three-dimensional integral equation in five variables, magnitudes of relative momenta and angles. This equation is solved through Padé summation. Based on a Malfliet-Tjon-type potential, the numerical feasibility and stability of the algorithm for solving the Faddeev equation is demonstrated. Special attention is given to the selection of independent variables and the treatment of three-body break-up singularities with a spline based method. The elastic differential cross section, semi-exclusive $d(N,N')$ cross sections and total cross sections of both elastic and breakup processes in the intermediate energy range up to about 1 GeV are calculated and the convergence of the multiple scattering series is investigated in every case. In general a truncation in the first or second order in the two-body t-matrix is quite insufficient.

PACS numbers: 21.45+v

I. INTRODUCTION

During the last two decades calculations of nucleon-deuteron scattering experienced large improvements and refinements. Here different techniques have been applied, Faddeev calculations in configuration space [1] and momentum space [2], and variational calculations based on a hyperspherical harmonic expansion [3, 4]. It is fair to say that below about 200 MeV projectile energy the momentum space Faddeev equations for three-nucleon scattering can now be solved with high accuracy for the most modern two- and three-nucleon forces. A summary for these achievements can be found in Ref. [5, 6, 7, 8, 9]. The approach described there is based on using angular momentum eigenstates for the two- and three-body systems. This partial wave decomposition replaces the continuous angle variables by discrete orbital angular momentum quantum numbers, and thus reduces the number of continuous variables to be discretized in a numerical treatment. For low projectile energies the procedure of considering orbital angular momentum components appears physically justified due to arguments related to the centrifugal barrier and the short range of the nuclear force. However, the algebraic and algorithmic steps to be carried out in a partial wave decomposition can be quite involved when solving the Faddeev equations. If one considers three-nucleon scattering at a few hundred MeV projectile energy, the number of partial waves needed to achieve convergence proliferates, and limitations with respect to computational feasibility and accuracy are reached.

It appears therefore natural to avoid a partial wave representation completely and work directly with vector variables. This is common practice in bound state calculations of few-nucleon systems based on variational [10] and Green's function Monte Carlo (GFMC) methods [11, 12, 13, 14], which are carried out in configuration space.

Our aim is to work directly with vector variables in the Faddeev scheme in momentum space. In earlier work [15, 16] we showed that the bound state Faddeev equation has a rather transparent structure when formulated with vector variables compared to the coupled set of two-dimensional integral equations obtained in a partial wave decomposed form. Based on Malfliet-Tjon type interactions for two- as well as three-body forces, it was demonstrated that the numerical solution of the bound state equation using vector variables is straightforward and numerically very accurate. As far as three nucleon scattering is concerned, the neutron-deuteron break-up process has been successfully studied up to 500 MeV projectile energy based on the first order term of the Faddeev equation using realistic nucleon-nucleon forces [17].

In this article we want to show that the full solution of the three-body scattering equation can be obtained in a straightforward manner when employing vector variables, i.e. magnitudes of momenta and angles between the momentum vectors. As a simplification we neglect spin and iso-spin degrees of freedom and treat three-boson scattering. The interactions employed are of Yukawa type, and no separable approximations are involved. The Faddeev equation for three identical bosons is solved exactly as function of momentum vectors below and above the three-body break-up.

This article is organized as follows. Section II reviews the Faddeev equation for three-body scattering in momentum

space and discusses our choice of momentum and angle variables for the unknown amplitude in the equation and its kernel. In Section III we derive the amplitudes and cross sections for elastic scattering and break-up processes. In addition we relate both via the optical theorem. In Section IV we discuss the numerical methods necessary for solving the Faddeev equation, especially our treatment of the singularities in the free three-body propagator. In addition, our numerical tests for the solution are shown and discussed. In Section V we present calculations for elastic scattering and break-up processes in the intermediate energy regime from 0.2 to 1 GeV. Our focus here is on the study of the importance of rescattering terms as function of the projectile energy and the reaction considered. We conclude in Section VI.

II. FADDEEV EQUATIONS FOR THREE BOSONS IN THE CONTINUUM

Various presentations of three-body scattering in the Faddeev scheme are presented in the literature [5, 6, 18]. We solve the Faddeev equation for three identical particles in the form

$$T|\phi\rangle = tP|\phi\rangle + tPG_0T|\phi\rangle. \quad (2.1)$$

The driving term of this integral equation consists of the two-body t -matrix t , the sum P of a cyclic and anticyclic permutation of three particles, and the initial state $|\phi\rangle = |\varphi_d\mathbf{q}_0\rangle$, composed of a two-body bound state and the momentum eigenstate of the projectile particle. The kernel of Eq. (2.1) contains the free three-body propagator, $G_0 = (E - H_0 + i\varepsilon)^{-1}$, where E is the total energy in the center of mass frame.

The operator T determines both, the full break-up amplitude

$$U_0 = (1 + P)T, \quad (2.2)$$

and the amplitude for elastic scattering

$$U = PG_0^{-1} + PT. \quad (2.3)$$

In this paper we focus on three identical bosons and use a momentum space representation. For solving Eq. (2.1), we introduce standard Jacobi momenta \mathbf{p} , the relative momentum in the subsystem, and \mathbf{q} , the relative momentum of the spectator to the subsystem. The momentum states are normalized according to $\langle \mathbf{p}'\mathbf{q}'|\mathbf{p}\mathbf{q}\rangle = \delta^3(\mathbf{p}' - \mathbf{p})\delta^3(\mathbf{q}' - \mathbf{q})$. Projecting Eq. (2.1) on to Jacobi momenta leads to [19]

$$\begin{aligned} \langle \mathbf{p}\mathbf{q}|T|\varphi_d\mathbf{q}_0\rangle &= \varphi_d \left(\mathbf{q} + \frac{1}{2}\mathbf{q}_0 \right) t_s \left(\mathbf{p}, \frac{1}{2}\mathbf{q} + \mathbf{q}_0, E - \frac{3}{4m}q^2 \right) \\ &+ \int d^3q'' t_s \left(\mathbf{p}, \frac{1}{2}\mathbf{q} + \mathbf{q}'', E - \frac{3}{4m}q^2 \right) \frac{\langle \mathbf{q} + \frac{1}{2}\mathbf{q}'', \mathbf{q}'' | T | \varphi_d\mathbf{q}_0 \rangle}{E - \frac{1}{m}(q^2 + q''^2 + \mathbf{q} \cdot \mathbf{q}'') + i\varepsilon}. \end{aligned} \quad (2.4)$$

Here $t_s(\mathbf{p}', \mathbf{p}) = t(\mathbf{p}, \mathbf{p}') + t(-\mathbf{p}', \mathbf{p})$ is the symmetrized t matrix and E is the total energy in the center of mass (c.m.) system

$$E = E_d + \frac{3}{4m}q_0^2 = E_d + \frac{2}{3}E_{lab}. \quad (2.5)$$

We assume that the underlying force is a two-body force, generating t via a two-body Lippmann-Schwinger equation and supporting one bound state with energy E_d . Thus, $t_s(z)$ has a pole at $z = E_d$. Since the transition operator T in Eq. (2.4) is needed for all values of \mathbf{q} , one encounters this pole of t_s . Extracting the residue explicitly by defining

$$t_s(\mathbf{p}', \mathbf{p}, z) \equiv \frac{\hat{t}_s(\mathbf{p}', \mathbf{p}, z)}{z - E_d} \quad (2.6)$$

and similarly for T , Eq. (2.4) can be rewritten as

$$\begin{aligned} \langle \mathbf{p}\mathbf{q}|\hat{T}|\varphi_d\mathbf{q}_0\rangle &= \varphi_d \left(\mathbf{q} + \frac{1}{2}\mathbf{q}_0 \right) \hat{t}_s \left(\mathbf{p}, \frac{1}{2}\mathbf{q} + \mathbf{q}_0, E - \frac{3}{4m}q^2 \right) \\ &+ \int d^3q'' \frac{\hat{t}_s \left(\mathbf{p}, \frac{1}{2}\mathbf{q} + \mathbf{q}'', E - \frac{3}{4m}q^2 \right)}{E - \frac{1}{m}(q^2 + q''^2 + \mathbf{q} \cdot \mathbf{q}'') + i\varepsilon} \frac{\langle \mathbf{q} + \frac{1}{2}\mathbf{q}'', \mathbf{q}'' | \hat{T} | \varphi_d\mathbf{q}_0 \rangle}{E - \frac{3}{4m}q''^2 - E_d + i\varepsilon}. \end{aligned} \quad (2.7)$$

This expression is the starting point for our numerical calculation of the transition amplitude without employing an angular momentum decomposition.

The first important step for an explicit calculation is the selection of independent variables. Since we ignore spin and iso-spin dependencies, the matrix element $\langle \mathbf{p}\mathbf{q}|\hat{T}|\varphi_d\mathbf{q}_0 \rangle$ is a scalar function of the variables \mathbf{p} and \mathbf{q} for a given projectile momentum \mathbf{q}_0 . Thus one needs 5 variables to uniquely specify the geometry of the three vectors \mathbf{p} , \mathbf{q} and \mathbf{q}_0 , which are shown in Fig. 1. Having in mind that with three vectors one can span 2 planes, i.e. the $\mathbf{p}\text{-}\mathbf{q}_0$ -plane and the $\mathbf{q}\text{-}\mathbf{q}_0$ -plane, a natural choice of independent variables is

$$p = |\mathbf{p}|, \quad q = |\mathbf{q}|, \quad x_p = \hat{\mathbf{p}} \cdot \hat{\mathbf{q}}_0, \quad x_q = \hat{\mathbf{q}} \cdot \hat{\mathbf{q}}_0, \quad x_{pq}^{q_0} = (\widehat{\mathbf{q}_0 \times \mathbf{q}}) \cdot (\widehat{\mathbf{q}_0 \times \mathbf{p}}). \quad (2.8)$$

The last variable, $x_{pq}^{q_0}$, is the angle between the two normal vectors of the $\mathbf{p}\text{-}\mathbf{q}_0$ -plane and the $\mathbf{q}\text{-}\mathbf{q}_0$ -plane, which are explicitly given by

$$\begin{aligned} (\widehat{\mathbf{q}_0 \times \mathbf{p}}) &= \frac{\hat{\mathbf{q}}_0 \times \hat{\mathbf{p}}}{\sqrt{1 - (\hat{\mathbf{q}}_0 \cdot \hat{\mathbf{p}})^2}}, \\ (\widehat{\mathbf{q}_0 \times \mathbf{q}}) &= \frac{\hat{\mathbf{q}}_0 \times \hat{\mathbf{q}}}{\sqrt{1 - (\hat{\mathbf{q}}_0 \cdot \hat{\mathbf{q}})^2}}. \end{aligned} \quad (2.9)$$

It should be pointed out, that the angle between the vectors \mathbf{q} and \mathbf{p} , $y_{pq} = \hat{\mathbf{p}} \cdot \hat{\mathbf{q}}$, is **not** an independent variable. In fact, if x_p and x_q are given, the domain of y_{pq} is bound by

$$x_p x_q - \sqrt{1 - x_p^2} \sqrt{1 - x_q^2} \leq y_{pq} \leq x_p x_q + \sqrt{1 - x_p^2} \sqrt{1 - x_q^2}, \quad (2.10)$$

thus not covering the entire interval $[-1,1]$. Using the explicit representation of the normal vectors and standard cross product identities, we arrive at the following relation between $x_{pq}^{q_0}$ and y_{pq} ,

$$\begin{aligned} x_{pq}^{q_0} &= \frac{\hat{\mathbf{p}} \cdot \hat{\mathbf{q}} - (\hat{\mathbf{q}}_0 \cdot \hat{\mathbf{p}})(\hat{\mathbf{q}}_0 \cdot \hat{\mathbf{q}})}{\sqrt{1 - (\hat{\mathbf{q}}_0 \cdot \hat{\mathbf{p}})^2} \sqrt{1 - (\hat{\mathbf{q}}_0 \cdot \hat{\mathbf{q}})^2}} \\ &= \frac{y_{pq} - x_p x_q}{\sqrt{1 - x_p^2} \sqrt{1 - x_q^2}}, \end{aligned} \quad (2.11)$$

or

$$y_{pq} = x_p x_q + \sqrt{1 - x_p^2} \sqrt{1 - x_q^2} x_{pq}^{q_0}. \quad (2.12)$$

For the special case where $\hat{\mathbf{q}}_0$ is parallel to the z -axis (q_0 -system) one can write

$$y_{pq} = x_p x_q + \sqrt{1 - x_p^2} \sqrt{1 - x_q^2} \cos \varphi_{pq}, \quad (2.13)$$

where the φ_{pq} is the difference of the azimuthal angles of $\hat{\mathbf{p}}$ and $\hat{\mathbf{q}}$. However, the variable $\cos \varphi_{pq}$, which was used erroneously in [19] as third angular variable, is not rotationally invariant.

With the independent variables listed in Eq. (2.8) the matrix element of \hat{T} is given as

$$\langle \mathbf{p}\mathbf{q}|\hat{T}|\varphi_d\mathbf{q}_0 \rangle \equiv \hat{T}(p, x_p, x_{pq}^{q_0}, x_q, q; q_0). \quad (2.14)$$

Furthermore, $\hat{t}_s(\mathbf{p}', \mathbf{p}, z)$ is also a scalar function, and thus can be written in the form

$$\hat{t}_s(\mathbf{p}', \mathbf{p}, z) = \hat{t}_s(p', p, \hat{\mathbf{p}}' \cdot \hat{\mathbf{p}}, z). \quad (2.15)$$

The most intricate dependence appears under the integral in Eq. (2.7) for the third angular variable of the \hat{T} -amplitude. According to Eq. (2.11) it is given as

$$x_{(q+\frac{1}{2}q'')q''}^{q_0} \equiv \frac{(\widehat{\mathbf{q} + \frac{1}{2}\mathbf{q}''}) \cdot \widehat{\mathbf{q}''} - \hat{\mathbf{q}}_0 \cdot (\widehat{\mathbf{q} + \frac{1}{2}\mathbf{q}''}) \hat{\mathbf{q}}_0 \cdot \widehat{\mathbf{q}''}}{\sqrt{1 - (\hat{\mathbf{q}}_0 \cdot (\widehat{\mathbf{q} + \frac{1}{2}\mathbf{q}''}))^2} \sqrt{1 - (\hat{\mathbf{q}}_0 \cdot \widehat{\mathbf{q}''})^2}}. \quad (2.16)$$

In view of the break-up singularities of the first denominator in Eq. (2.7) it is mandatory to choose the coordinate system for the \mathbf{q}'' -integration such that the z-axis points parallel to the vector $\hat{\mathbf{q}}$. Then one obtains for Eq. (2.16)

$$x_{(q+\frac{1}{2}q'')q''}^{q_0} = \frac{\frac{qx''+\frac{1}{2}q''}{\sqrt{q^2+\frac{1}{4}q''^2+qq''x''}} - x_{q+\frac{1}{2}q''}x_{q''}}{\sqrt{1-x_{q+\frac{1}{2}q''}^2}\sqrt{1-x_{q''}^2}}, \quad (2.17)$$

where

$$\begin{aligned} x_{q''} &\equiv \hat{\mathbf{q}}'' \cdot \hat{\mathbf{q}}_0 = x''x_q + \sqrt{1-x''^2}\sqrt{1-x_q^2} \cos(\varphi'' - \varphi_{q_0}) \\ x_{q+\frac{1}{2}q''} &\equiv (\mathbf{q} + \frac{1}{2}\mathbf{q}'') \cdot \hat{\mathbf{q}}_0 = \frac{qx_q + \frac{1}{2}q''x_{q''}}{\sqrt{q^2 + \frac{1}{4}q''^2 + qq''x''}}. \end{aligned} \quad (2.18)$$

Here φ_{q_0} is the azimuthal angle of $\hat{\mathbf{q}}_0$ in the coordinate system chosen for the \mathbf{q}'' -integration. These considerations lead to the explicit representation for the transition amplitude \hat{T}

$$\begin{aligned} \hat{T}(p, x_p, x_{pq}^{q_0}, x_q, q; q_0) &= \varphi_d \left(\sqrt{q^2 + \frac{1}{4}q_0^2 + qq_0x_q} \right) \\ &\times \hat{t}_s \left(p, \sqrt{\frac{1}{4}q^2 + q_0^2 + qq_0x_q}, \frac{\frac{1}{2}qy_{pq} + q_0x_p}{\sqrt{\frac{1}{4}q^2 + q_0^2 + qq_0x_q}}; E - \frac{3}{4m}q^2 \right) \\ &+ \int_0^\infty dq'' q''^2 \int_{-1}^{+1} dx'' \int_0^{2\pi} d\varphi'' \frac{1}{E - \frac{1}{m}(q^2 + qq''x'' + q''^2) + i\varepsilon} \\ &\times \hat{t}_s \left(p, \sqrt{\frac{1}{4}q^2 + q''^2 + qq''x''}, \frac{\frac{1}{2}qy_{pq} + q''y_{pq''}}{\sqrt{\frac{1}{4}q^2 + q''^2 + qq''x''}}; E - \frac{3}{4m}q^2 \right) \\ &\times \frac{\hat{T} \left(\sqrt{q^2 + \frac{1}{4}q''^2 + qq''x''}, \frac{qx_q + \frac{1}{2}q''x_{q''}}{\sqrt{q^2 + \frac{1}{4}q''^2 + qq''x''}}, \frac{\frac{qx''+\frac{1}{2}q''}{\sqrt{q^2+\frac{1}{4}q''^2+qq''x''}} - x_{q+\frac{1}{2}q''}x_{q''}}{\sqrt{1-x_{q+\frac{1}{2}q''}^2}\sqrt{1-x_{q''}^2}}, x_{q''}, q''; q_0 \right)}{E - \frac{3}{4m}q''^2 - E_d + i\varepsilon} \end{aligned} \quad (2.19)$$

where in addition to Eq. (2.8) and the related variables of Eq. (2.12) and Eq. (2.18) the following variables occur

$$\begin{aligned} q'' &= |\mathbf{q}''|, \\ x'' &= \hat{\mathbf{q}} \cdot \hat{\mathbf{q}}'', \\ y_{pq''} &= \hat{\mathbf{p}} \cdot \hat{\mathbf{q}}'' = y_{pq}x'' + \sqrt{1-x''^2}\sqrt{1-y_{pq}^2} \cos(\varphi_p - \varphi''). \end{aligned} \quad (2.20)$$

Like φ_{q_0} in Eq. (2.18), the angle φ_p in Eq. (2.20) is the azimuthal angle of $\hat{\mathbf{p}}$ in the q -system (i.e. the system where the z-axis is parallel to $\hat{\mathbf{q}}$). It remains to relate the angles φ_p and φ_{q_0} to the three angular variables x_p , x_q , and $x_{pq}^{q_0}$. As it is shown in Appendix A, due to the φ'' -integration, only the knowledge of $\cos(\varphi_p - \varphi_{q_0})$ is required. Like $\cos \varphi_{pq}$ in Eq. (2.13) is equal to $x_{pq}^{q_0}$ in the q_0 -system, so is $\cos(\varphi_p - \varphi_{q_0})$ equal to $x_{q_0 p}^q$ in the q -system. Thus

$$\cos(\varphi_p - \varphi_{q_0}) = x_{q_0 p}^q = \frac{\hat{\mathbf{q}}_0 \cdot \hat{\mathbf{p}} - (\hat{\mathbf{q}} \cdot \hat{\mathbf{q}}_0)(\hat{\mathbf{q}} \cdot \hat{\mathbf{p}})}{\sqrt{1 - (\hat{\mathbf{q}} \cdot \hat{\mathbf{q}}_0)^2}\sqrt{1 - (\hat{\mathbf{p}} \cdot \hat{\mathbf{q}})^2}} = \frac{x_p - x_q y_{pq}}{\sqrt{1 - x_q^2}\sqrt{1 - y_{pq}^2}}. \quad (2.21)$$

Because of that difference $(\varphi_p - \varphi_{q_0})$, one can choose φ_{q_0} arbitrarily, e.g. zero. Furthermore, $\cos \varphi_p$ and $\sin \varphi_p$ required in Eq. (2.20) are given in terms of $\cos(\varphi_p - \varphi_{q_0})$, as is shown in Appendix A. This completes the definition of all relevant variables in Eq. (2.19).

III. AMPLITUDES AND CROSS SECTIONS FOR ELASTIC SCATTERING AND BREAK-UP PROCESSES

The amplitude for elastic scattering is obtained by calculating the matrix element of the operator U given in Eq. (2.3) as.

$$\begin{aligned} \langle \mathbf{q}\varphi_d | U | \mathbf{q}_0\varphi_d \rangle &= 2\varphi_d \left(\frac{1}{2}\mathbf{q} + \mathbf{q}_0 \right) \left(E - \frac{1}{m}(q^2 + \mathbf{q} \cdot \mathbf{q}_0 + q_0^2) \right) \varphi_d \left(\mathbf{q} + \frac{1}{2}\mathbf{q}_0 \right) \\ &+ 2 \int d^3q'' \varphi_d \left(\frac{1}{2}\mathbf{q} + \mathbf{q}'' \right) \frac{\langle \mathbf{q} + \frac{1}{2}\mathbf{q}'', \mathbf{q}'' | \hat{T} | \mathbf{q}_0\varphi_d \rangle}{E - \frac{3}{4m}q''^2 - E_d + i\varepsilon}. \end{aligned} \quad (3.1)$$

The amplitude for the full break-up process according to Eq. (2.2), is given by

$$\langle \mathbf{p}\mathbf{q} | U_0 | \mathbf{q}_0\varphi_d \rangle = \frac{\langle \mathbf{p}\mathbf{q} | \hat{T} | \mathbf{q}_0\varphi_d \rangle}{E - \frac{3}{4m}\mathbf{q}^2 - E_d} + \frac{\langle -\frac{1}{2}\mathbf{p} + \frac{3}{4}\mathbf{q}, -\mathbf{p} - \frac{1}{2}\mathbf{q} | \hat{T} | \mathbf{q}_0\varphi_d \rangle}{E - \frac{3}{4m}(-\mathbf{p} - \frac{1}{2}\mathbf{q})^2 - E_d} + \frac{\langle -\frac{1}{2}\mathbf{p} - \frac{3}{4}\mathbf{q}, +\mathbf{p} - \frac{1}{2}\mathbf{q} | \hat{T} | \mathbf{q}_0\varphi_d \rangle}{E - \frac{3}{4m}(+\mathbf{p} - \frac{1}{2}\mathbf{q})^2 - E_d} \quad (3.2)$$

The equation for the elastic operator U follows from Eqs. (2.1) and (2.3). It is given as

$$U|\phi\rangle = PG_0^{-1}|\phi\rangle + PtG_0U|\phi\rangle \quad (3.3)$$

Straightforward and well known steps [5] based on this equation lead to the unitarity relation

$$\begin{aligned} \langle \phi | U | \phi' \rangle^* - \langle \phi' | U | \phi \rangle &= \int d^3q \langle \phi_q | U | \phi' \rangle^* 2\pi i \delta(E - E_d - \frac{3}{4m}q^2) \langle \phi_q | U | \phi \rangle \\ &+ \frac{1}{3} \int d^3p d^3q \langle \phi_0 | U_0 | \phi' \rangle^* 2\pi i \delta(E - \frac{p^2}{m} - \frac{3}{4m}q^2) \langle \phi_0 | U_0 | \phi \rangle. \end{aligned} \quad (3.4)$$

We want to point out that there is a misprint in Eq. (202) of Ref. [5], the factor 1/3 is missing.

Using the variables defined in the previous section, and having in mind that for elastic scattering $|\mathbf{q}| = |\mathbf{q}_0|$, the amplitude for elastic scattering according to Eq. (3.1) can be expressed as

$$\begin{aligned} \langle \mathbf{q}\varphi_d | U | \mathbf{q}_0\varphi_d \rangle &\equiv U(q_0, x_q) = 2\varphi_d^2 \left(q_0 \sqrt{\frac{5}{4} + x_q} \right) \left(E - \frac{q_0^2}{m}(2 + x_q) \right) \\ &+ 2 \int_0^\infty dq'' q''^2 \int_{-1}^{+1} dx'' \int_0^{2\pi} d\varphi'' \frac{1}{E - \frac{3}{4m}q''^2 - E_d + i\varepsilon} \\ &\times \varphi_d \left(\sqrt{\frac{1}{4}q_0^2 + q''^2 + q_0 q'' y_{qq''}} \right) \\ &\times \hat{T} \left(\sqrt{q_0^2 + \frac{1}{4}q''^2 + q_0 q'' y_{qq''}}, \frac{q_0 x_q + \frac{1}{2}q'' y_{q_0 q''}}{\sqrt{q_0^2 + \frac{1}{4}q''^2 + q_0 q'' y_{qq''}}}, \frac{\frac{q_0 y_{qq''} + \frac{1}{2}q''}{\sqrt{q_0^2 + \frac{1}{4}q''^2 + q_0 q'' y_{qq''}}} - x_{\pi_p} x_{\pi_q}}{\sqrt{1 - x_{\pi_p}^2} \sqrt{1 - x_{\pi_q}^2}}, y_{q_0 q''}, q''; q_0 \right) \end{aligned} \quad (3.5)$$

with

$$\begin{aligned} y_{qq''} &= \hat{\mathbf{q}} \cdot \hat{\mathbf{q}}'' \\ y_{q_0 q''} &= \hat{\mathbf{q}}_0 \cdot \hat{\mathbf{q}}'' = x_{\pi_q} \\ x_{\pi_p} &= \frac{q_0 x_q + \frac{1}{2}q'' y_{q_0 q''}}{\sqrt{q_0^2 + \frac{1}{4}q''^2 + q_0 q'' y_{qq''}}}, \end{aligned} \quad (3.6)$$

At this point, the choice of a specific coordinate system for the \mathbf{q}'' -integration is still open. The angular variable $x_q = \hat{\mathbf{q}} \cdot \hat{\mathbf{q}}_0$ represents the scattering angle. If the z-axis is chosen parallel to $\hat{\mathbf{q}}_0$, the angles are

$$\begin{aligned} y_{qq''} &= x_q x'' + \sqrt{1 - x_q^2} \sqrt{1 - x''^2} \cos(\varphi_q - \varphi''). \\ y_{q_0 q''} &= x'' \end{aligned} \quad (3.7)$$

While having the z-axis parallel to $\hat{\mathbf{q}}_0$ may be the intuitive choice to describe the scattering with a given beam direction, we can in principle also choose the z-axis parallel to $\hat{\mathbf{q}}$. In that case the angles in Eq. (3.6) are given by

$$\begin{aligned} y_{qq''} &= x'' \\ y_{q_0q''} &= x_q x'' + \sqrt{1 - x_q^2} \sqrt{1 - x''^2} \cos(\varphi_{q_0} - \varphi''). \end{aligned} \quad (3.8)$$

The elastic cross section depends on the angle between the vectors $\hat{\mathbf{q}}_0$ and $\hat{\mathbf{q}}$, but not on the choice of z-axis. We use the possibility of calculating the matrix elements of U in the two different coordinate systems to test the quality of our numerical calculations.

The differential elastic cross section in the c.m. frame is given by

$$\frac{d\sigma_{el}}{d\Omega} = \left(\frac{2m}{3}\right)^2 (2\pi)^4 |U(q_0 x_q)|^2, \quad (3.9)$$

and the corresponding total elastic cross section is

$$\sigma_{el} = \int d\Omega \frac{d\sigma_{el}}{d\Omega} = \left(\frac{2m}{3}\right)^2 (2\pi)^5 \int_{-1}^{+1} dx |U(q_0, x)|^2. \quad (3.10)$$

The full break-up amplitude is given in Eq. (3.2). On the energy shell p and q are constrained by $p^2 + \frac{3}{4}q^2 = mE$. As function of all five variables and the projectile momentum it reads

$$U_0(p, x_p, x_{pq}^{q_0}, x_q, q, q_0) = \frac{\hat{T}(p, x_p, x_{pq}^{q_0}, x_q, q, q_0)}{E - \frac{3}{4m}q^2 - E_d} + \frac{\hat{T}(p_2, x_{p_2}, x_{p_2q_2}^{q_0}, x_{q_2}, q_2, q_0)}{E - \frac{3}{4m}q_2^2 - E_d} + \frac{\hat{T}(p_3, x_{p_3}, x_{p_3q_3}^{q_0}, x_{q_3}, q_3, q_0)}{E - \frac{3}{4m}q_3^2 - E_d}. \quad (3.11)$$

Here the variables are defined as

$$\begin{aligned} y_{pq} &= x_p x_q + \sqrt{1 - x_p^2} \sqrt{1 - x_q^2} x_{pq}^{q_0} \\ p_2 &= \left| -\frac{1}{2}\mathbf{p} + \frac{3}{4}\mathbf{q} \right| = \frac{1}{2} \sqrt{p^2 + \frac{9}{4}q^2 - 3pqy_{pq}} \\ q_2 &= \left| -\mathbf{p} - \frac{1}{2}\mathbf{q} \right| = \sqrt{p^2 + \frac{1}{4}q^2 + pqy_{pq}} \\ p_3 &= \left| -\frac{1}{2}\mathbf{p} - \frac{3}{4}\mathbf{q} \right| = \frac{1}{2} \sqrt{p^2 + \frac{9}{4}q^2 + 3pqy_{pq}} \\ q_3 &= \left| +\mathbf{p} - \frac{1}{2}\mathbf{q} \right| = \sqrt{p^2 + \frac{1}{4}q^2 - pqy_{pq}} \\ x_{p_2} &= \hat{\mathbf{p}}_2 \cdot \hat{\mathbf{q}}_0 = \frac{-\frac{1}{2}px_p + \frac{3}{4}qx_q}{p_2} \\ x_{q_2} &= \hat{\mathbf{q}}_2 \cdot \hat{\mathbf{q}}_0 = \frac{-px_p - \frac{1}{2}qx_q}{q_2} \\ x_{p_3} &= \hat{\mathbf{p}}_3 \cdot \hat{\mathbf{q}}_0 = \frac{-\frac{1}{2}px_p - \frac{3}{4}qx_q}{p_3} \\ x_{q_3} &= \hat{\mathbf{q}}_3 \cdot \hat{\mathbf{q}}_0 = \frac{+px_p - \frac{1}{2}qx_q}{q_3} \\ x_{p_2q_2}^{q_0} &= (\hat{\mathbf{q}}_0 \times \hat{\mathbf{p}}_2) \cdot (\hat{\mathbf{q}}_0 \times \hat{\mathbf{q}}_2) = \frac{\frac{1}{2}p^2 - \frac{3}{8}q^2 - \frac{1}{2}pqy_{pq}}{\sqrt{1 - x_{p_2}^2} \sqrt{1 - x_{q_2}^2}} - x_{p_2} x_{q_2} \\ x_{p_3q_3}^{q_0} &= (\hat{\mathbf{q}}_0 \times \hat{\mathbf{p}}_3) \cdot (\hat{\mathbf{q}}_0 \times \hat{\mathbf{q}}_3) = \frac{-\frac{1}{2}p^2 + \frac{3}{8}q^2 - \frac{1}{2}pqy_{pq}}{\sqrt{1 - x_{p_3}^2} \sqrt{1 - x_{q_3}^2}} - x_{p_3} x_{q_3} \end{aligned} \quad (3.12)$$

The five-fold differential break-up cross section is given in the c.m. frame

$$\frac{d^5\sigma_{br}}{d\Omega_p d\Omega_q dq} = \frac{(2\pi)^4 m^2}{3q_0} q^2 \sqrt{mE - \frac{3}{4}q^2} |U_0(p, x_p, x_{pq}^{q_0}, x_q, q, q_0)|^2 \quad (3.13)$$

It is convenient to calculate the total break-up cross section in the c.m. frame, since there are no kinematic restrictions on the relative angles. For the explicit calculation we can make different choices of the z-axis, e.g. it can be parallel to the direction $\hat{\mathbf{q}}_0$ of the projectile, or parallel to either one of the Jacobi vectors $\hat{\mathbf{q}}$ and $\hat{\mathbf{p}}$. The different choices will obviously result in different angular integrations. For completeness we give all three choices here. This will be used as a highly non-trivial test of the numerical results, as will be demonstrated in the next Section. If the z-axis is parallel to $\hat{\mathbf{q}}_0$ we have

$$\int d\Omega_p d\Omega_q = 2\pi \int_{-1}^{+1} dx_p'' \int_{-1}^{+1} dx_q'' \int_0^{2\pi} d\varphi_{pq}'' \quad (3.14)$$

with

$$x_p \rightarrow x_p'', \quad x_q \rightarrow x_q'', \quad x_{pq}^{q_0} \rightarrow \cos \varphi_{pq}'' \quad (3.15)$$

If the z-axis is parallel to $\hat{\mathbf{q}}$, the angular integration becomes

$$\int d\Omega_p d\Omega_q = 2\pi \int_{-1}^{+1} dx_q'' \int_{-1}^{+1} dy_{pq}'' \int_0^{2\pi} d\varphi_{pq}'' \quad (3.16)$$

with

$$\begin{aligned} x_p &\rightarrow x_q'' y_{pq}'' + \sqrt{1 - x_q''^2} \sqrt{1 - y_{pq}''^2} \cos \varphi_{pq}'' , \\ x_q &\rightarrow x_q'' , \\ x_{pq}^{q_0} &\rightarrow \frac{y_{pq}'' - (x_q'' y_{pq}'' + \sqrt{1 - x_q''^2} \sqrt{1 - y_{pq}''^2} \cos \varphi_{pq}'') x_q''}{\sqrt{1 - (x_q'' y_{pq}'' + \sqrt{1 - x_q''^2} \sqrt{1 - y_{pq}''^2} \cos \varphi_{pq}'')^2} \sqrt{1 - x_q''^2}} . \end{aligned} \quad (3.17)$$

Finally, if the z-axis is parallel to $\hat{\mathbf{p}}$, the angular integration is

$$\int d\Omega_p d\Omega_q = 2\pi \int_{-1}^{+1} dx_p'' \int_{-1}^{+1} dy_{pq}'' \int_0^{2\pi} d\varphi_{qq_0}'' \quad (3.18)$$

with

$$\begin{aligned} x_p &\rightarrow x_p'' , \\ x_q &\rightarrow x_p'' y_{pq}'' + \sqrt{1 - x_p''^2} \sqrt{1 - y_{pq}''^2} \cos \varphi_{qq_0}'' , \\ x_{pq}^{q_0} &\rightarrow \frac{y_{pq}'' - (x_p'' y_{pq}'' + \sqrt{1 - x_p''^2} \sqrt{1 - y_{pq}''^2} \cos \varphi_{qq_0}'') x_p''}{\sqrt{1 - (x_p'' y_{pq}'' + \sqrt{1 - x_p''^2} \sqrt{1 - y_{pq}''^2} \cos \varphi_{qq_0}'')^2} \sqrt{1 - x_p''^2}} . \end{aligned} \quad (3.19)$$

Let us define a function $\mathcal{F}(p, q)$ as

$$\mathcal{F}(p, q) = \int d\Omega_p d\Omega_q |\langle \phi_0 | U_0 | \phi \rangle|^2 , \quad (3.20)$$

where the angle integrations over the break-up amplitude is carried out. This function should be independent of the coordinate system in which the angle integrations are performed. We use this property to check our numerical calculations. This is a non-trivial test of our calculation, since especially at higher energies the transition amplitude \hat{T} develops stronger angle dependencies, which challenge the accuracy of the multi-dimensional interpolations.

The angle integrated break-up cross section is given as

$$\frac{d\sigma_{br}}{dq} = \frac{1}{3} \frac{(2\pi)^4 m^2}{3q_0} q^2 \sqrt{mE - \frac{3}{4}q^2} \mathcal{F} \left(\sqrt{mE - \frac{3}{4}q^2}, q \right) , \quad (3.21)$$

and the total break-up cross section reads

$$\sigma_{br} = \frac{1}{3} \frac{(2\pi)^4 m^2}{3q_0} \int_0^{\sqrt{\frac{4mE}{3}}} dq q^2 \sqrt{mE - \frac{3}{4}q^2} \mathcal{F} \left(\sqrt{mE - \frac{3}{4}q^2}, q \right) . \quad (3.22)$$

Using now the unitarity relation from Eq. (3.4) the optical theorem gives

$$\sigma_{tot} = \sigma_{el} + \sigma_{br} = -\frac{4m(2\pi)^3}{3q_0} \text{Im}U(q_0, 1). \quad (3.23)$$

For later use we also mention the semi-exclusive cross section, where only one particle is detected in the break-up process

$$\frac{d\sigma}{d\Omega_q dq} = (2\pi)^4 \frac{m^2}{3q_0} pq^2 \int d\hat{p} |U_0(p, x_p, x_{pq}^{q_0}, x_q, q, q_0)|^2 \quad (3.24)$$

IV. NUMERICAL METHODS

The fully off-shell two-body t-matrix $t(\mathbf{p}', \mathbf{p}, z)$ is solved directly from the Lippmann-Schwinger equation as function of its vector variables [20] for the off-shell energies $E - \frac{3}{4m}q^2$ as required by Eq. (2.4). The Faddeev equation is iterated, generating the multiple scattering series, which is then summed by the Padé method [21, 22]. We use it in the form of a continued fraction expansion as layed out in Ref. [18].

The first integration to be performed in solving Eq. (2.19) by iteration is the integration over the azimuthal angle φ'' . This leads to a function of variables, q'' and x'' and requires interpolation in the second and third arguments of t_s and the first four arguments of \hat{T} . Our spline interpolations are based on the cubic Hermite splines given in [23].

Let $F(q'', x'')$ be the resulting function in each step of the iteration. Clearly, it depends in addition on the fixed variables p , q , x_p , x_q , and $x_{pq}^{q_0}$, which are omitted for clarity. Then the next task is performing the remaining two singular integrations,

$$I = \int_0^\infty dq'' q''^2 \int_{-1}^{+1} dx'' \frac{F(q'', x'')}{(E - \frac{1}{m}(q^2 + q''^2 + qq''x'') + i\varepsilon)(E - \frac{3}{4m}q''^2 - E_d + i\varepsilon)} \quad (4.1)$$

If the c.m. energy E is below the three-body break-up threshold, only the second denominator is singular, and the simple pole can be treated by standard subtraction methods.

The intricate problem arises above the three-body break-up threshold, when in addition the first denominator can vanish. It has the form

$$\frac{1}{E - \frac{1}{m}(q^2 + qq''x'' + q''^2) + i\varepsilon} = \frac{\frac{m}{qq''}}{x_0 - x'' + i\varepsilon} \quad (4.2)$$

with

$$x_0 = \frac{mE - q^2 - q''^2}{qq''}. \quad (4.3)$$

For $|x_0| \leq 1$ a so-called moving singularity arises in the q'' - x'' -integration, since x_0 depends on q . The direct treatment of those moving singularities using real variables has been discussed in the literature [2]. We briefly review the appearance of these singularities in form of logarithms, since we introduce a new quasi-analytic integration based on Spline functions. The condition $|x_0| = 1$ leads to the pole positions

$$q'' = \pm \frac{q}{2} \pm \sqrt{mE - \frac{3}{4}q^2}, \quad (4.4)$$

and one arrives at the well known shape in the q - q'' -plane for $|x_0| \leq 1$ shown in Fig. 2. This region is bounded by

$$q_+ = \frac{q}{2} + \sqrt{Q_0^2 - \frac{3}{4}q^2} \quad (4.5)$$

and

$$q_- = \begin{cases} -\frac{q}{2} + \sqrt{Q_0^2 - \frac{3}{4}q^2} & q < Q_0 \\ +\frac{q}{2} - \sqrt{Q_0^2 - \frac{3}{4}q^2} & q > Q_0 \end{cases} \quad (4.6)$$

where $Q_0 = \sqrt{mE}$. Apparently there is no singularity if $q > q_{max} \equiv \sqrt{\frac{4m}{3}E}$. We distinguish four cases, $q = 0$, $0 < q < q_{max}$, $q = q_{max}$, and $q > q_{max}$. The case $q = 0$ reduces to a simple subtraction and will not be discussed. For $0 < q < q_{max}$ we only consider the part of the q'' -integration which contains the moving singularities. It has the schematic form

$$I' = \int_0^{q_{max}} dq'' \int_{-1}^{+1} dx'' \frac{f(q'', x'')}{x_0 - x'' + i\varepsilon}. \quad (4.7)$$

The first step is to perform a subtraction of the pole, which we carry out in the entire square $0 \leq q, q'' \leq q_{max}$ by defining

$$\hat{f}(q'', x_0) = \begin{cases} f(q'', x_0) : |x_0| \leq 1 \\ f(q'', \frac{x_0}{|x_0|}) : |x_0| > 1 \end{cases} \quad (4.8)$$

We obtain

$$\begin{aligned} I' &= \int_0^{q_{max}} dq'' \int_{-1}^{+1} dx'' \frac{f(q'', x'') - \hat{f}(q'', x_0)}{x_0 - x''} \\ &+ \int_0^{q_{max}} dq'' \hat{f}(q'', x_0) \ln \left| \frac{1+x_0}{1-x_0} \right| - i\pi \int_0^{q_{max}} dq'' \Theta(1-|x_0|) \hat{f}(q'', x_0). \end{aligned} \quad (4.9)$$

Now we define $q_- = \frac{q}{2} - \sqrt{Q_0^2 - \frac{3}{4}q^2}$ and obtain

$$\ln \left| \frac{1+x_0}{1-x_0} \right| = \left(-\frac{q_-}{|q_-|} \ln |q'' + |q_-|| - \ln |q'' + q_+| \right) + \left(+\frac{q_-}{|q_-|} \ln |q'' - |q_-|| + \ln |q'' - q_+| \right). \quad (4.10)$$

This leads to the well separated part of the integral which contains the logarithmic singularity

$$\int_0^{q_{max}} dq'' \hat{f}(q'', x_0) \left(+\frac{q_-}{|q_-|} \ln |q'' - |q_-|| + \ln |q'' - q_+| \right). \quad (4.11)$$

It is here that we introduce the new technique that relies on cubic spline integration.

We divide the range of integration $[0, q_{max}]$ into intervals bounded by a set of grid points q_i . The set of grid points is supposed to be dense enough to interpolate the function $\hat{f}(q'', x_0) \equiv f(q'')$ sufficiently well by cubic Hermitean splines [23]. In Ref. [23] a detailed presentation of these spline functions is given specific for our use. For the convenience of the reader we now switch to the notation of [23] and denote the end points of the i -th interval by x_1 and x_2 and the two adjacent grid points to the left and right of the i -th interval by x_0 and x_3 , respectively. Then as detailed in [23] the interpolating function in the i -th interval (replacing $f(q'') \equiv f(x)$) can be written as

$$f_i(x) = \sum_{j=0}^3 S_j(x) f(x_j), \quad (4.12)$$

where the modified spline functions are

$$\begin{aligned} S_0(x) &= -\phi_3(x) \frac{x_2 - x_1}{x_1 - x_0} \frac{1}{x_2 - x_0}, \\ S_1(x) &= \phi_1(x) + \phi_3 \left(\frac{x_2 - x_1}{x_1 - x_0} - \frac{x_1 - x_0}{x_2 - x_1} \right) \frac{1}{x_2 - x_0} - \phi_4(x) \frac{x_3 - x_2}{x_2 - x_1} \frac{1}{x_3 - x_1}, \\ S_2(x) &= \phi_2(x) + \phi_3 \frac{x_1 - x_0}{x_2 - x_1} \frac{1}{x_2 - x_0} + \phi_4(x) \left(\frac{x_3 - x_2}{x_2 - x_1} - \frac{x_2 - x_1}{x_3 - x_2} \right) \frac{1}{x_3 - x_1}, \\ S_3(x) &= \phi_4(x) \frac{x_2 - x_1}{x_3 - x_2} \frac{1}{x_3 - x_1}. \end{aligned} \quad (4.13)$$

with

$$\phi_1(x) = \frac{(x_2 - x)^2}{(x_2 - x_1)^3} [(x_2 - x_1) + 2(x - x_1)],$$

$$\begin{aligned}
\phi_2(x) &= \frac{(x_1 - x)^2}{(x_2 - x_1)^3} [(x_2 - x_1) + 2(x_2 - x)], \\
\phi_3(x) &= \frac{(x - x_1)(x_2 - x)^2}{(x_2 - x_1)^2}, \\
\phi_4(x) &= \frac{(x - x_1)^2(x - x_2)}{(x_2 - x_1)^2}.
\end{aligned} \tag{4.14}$$

Therefore, in view of Eqs. (4.11)- (4.14), the following integrals occur for $i = 1 \dots 4$

$$\begin{aligned}
\bar{\phi}_1 &= \int_{x_i}^{x_{i+1}} \phi_1 \ln |x - q| dx, \\
\bar{\phi}_2 &= \int_{x_i}^{x_{i+1}} \phi_2 \ln |x - q| dx, \\
\bar{\phi}_3 &= \int_{x_i}^{x_{i+1}} \phi_3 \ln |x - q| dx, \\
\bar{\phi}_4 &= \int_{x_i}^{x_{i+1}} \phi_4 \ln |x - q| dx.
\end{aligned} \tag{4.15}$$

with $q = |q_-|, q_+$. Consequently the five different cases $q < x_i < x_{i+1}$, $q = x_i < x_{i+1}$, $x_i < q < x_{i+1}$, $x_i < q = x_{i+1}$, and $x_i < x_{i+1} < q$ occur. Since the functions $\phi_i(x)$ are cubic polynomials, the integrals in Eq. (4.15) can be performed analytically. We leave the explicit calculation to interested practitioner and refer to [24] for a detailed presentation. According to our experience that manner to integrate the moving logarithmic singularities is a very good alternative to the more common subtraction method [2].

Finally, for $q = q_{max}$ we also apply the subtraction over the extended region $0 \leq q'' \leq q_{max}$. In that case $q_+ = q_- = \frac{q_{max}}{2}$ and when $q'' = \frac{q_{max}}{2}$ then $x_0 = -1$. Analogous steps lead to that part of the integral, which contains the logarithmic singularity,

$$\int_0^{q_{max}} dq'' \hat{f}(q'', -1) \ln \left| q'' - \frac{q_{max}}{2} \right|, \tag{4.16}$$

which is again evaluated by spline based integration.

In order to test the correctness as well as the accuracy of our calculations we carried out a variety of numerical tests. Unfortunately we could not compare to work by other groups, since to the best of our knowledge no comparable work at higher energies exists.

Apart from the projectile momentum q_0 , the amplitude \hat{T} of Eq. (2.19) depends on five variables p , x_p , $x_{pq}^{q_0}$, x_q , and q . In addition, there are the integration variables q'' , x'' and φ'' . All calculations listed are based on the Malfliet-Tjon type potential which is explicitly given in the next section. The fully off-shell two-body t -matrix, $t(p', p, x, \varepsilon)$, is obtained for each fixed energy on a symmetric momentum grid with 60 p (p') points and 40 x points. Since the momentum region which contributes to a solution of the two-body t -matrix is quite different from the region of importance in a three-body calculation, we map our solution for t_s onto the momentum grid relevant for the three-body transition amplitude. This is done by applying the Lippmann-Schwinger equation repeatedly. The t -matrix $t_s(p', p, x, \varepsilon)$ is obtained at energies $\varepsilon = E - \frac{3}{4m}q^2$, exactly at the q values needed in the three-body transition amplitude of Eq. (2.19).

In Table I the differential elastic cross section at selected angles and two energies is shown together with various grid points used in the calculation. In Table II the total elastic, the total breakup as well as the total cross section evaluated according to Eq. (3.23) via the optical theorem are given calculated as function of various sets of grid points. The momentum grids for p and q are discretized with 49 points each. The integration variable q'' plays the same role as q , and is therefore also discretized with 49 points. Both tables show that the angular dependence at the low energy, 0.01 GeV, is very weak, and in principle 12 grid points are sufficient for all angles. This is quite different at 0.5 GeV, where 16 angle points are clearly insufficient for x_p , x_q , and x'' . Only $x_{pq}^{q_0}$ and φ'' exhibit a weaker angular dependence, and 13 to 18 grid points are enough. It turns out that with 20 points for x_p and 24 points for x_q and x'' we obtain converged calculations when considering the differential cross section at selected angles in Table I and the total cross sections in Table II. The calculations at higher energies presented in the following are based on the grid given in the last row of Table II. This grid allows sufficiently accurate calculations over the wide energy range considered.

A nontrivial test for the quality accuracy of our calculation is the numerical verification of the optical theorem Eq. (3.23). Our results are given for selected energies in Table III. Here we show two sets of cross sections, distinguished

by the superscripts q_0 and q . The superscripts indicate that the calculation is carried out by choosing the z-axis either parallel to $\hat{\mathbf{q}}_0$ or to $\hat{\mathbf{q}}$. Performing the calculation with two different choices of the z-axis is a nontrivial test for our choice of independent variables as well as for the entire calculation. The calculations are based on the standard grid given above and show a very good agreement of the results obtained in the two different coordinate systems, indicating the numerical rotational invariance of our calculations.

On top of convergence tests for the Padé summation, we insert the resulting amplitude \hat{T} again into the integral of Eq. (2.19), leading to a second amplitude \hat{T}' . Both amplitudes should be identical within our numerical errors. This is checked by evaluating the cross sections again using the second amplitude. We document the results in Table IV for the differential elastic cross section at selected angles. The table shows excellent agreement of the two values of the cross section

Finally, another highly nontrivial test of our calculation is the independence of the cross sections from the arbitrary angle φ_{q_0} and the sign of $\sin(\varphi_p - \varphi_{q_0})$. This is documented in Tables V and VI for the energy $E=3$ MeV. In order to check the rotational invariance numerically, the calculations are carried out in two different coordinate systems, one where \mathbf{q}_0 is parallel the z -axis, and one where \mathbf{q} is parallel to z . Both tables show excellent agreement for the cross sections, and thus we conclude that our choice of variables is correct.

V. SCATTERING CALCULATIONS AT INTERMEDIATE ENERGIES

Through we neglect spin and iso-spin degrees of freedom and stay in a strictly nonrelativistic framework, we nevertheless can provide first qualitative insights for various cross sections in three-body scattering in the intermediate energy regime which we define from 200 MeV to 1 GeV projectile energy. The focus of our investigations will be the question which orders of rescattering in the two-body t -matrix are needed to come close to the exact result, namely the solution of the Faddeev equation.

As a model two-body interaction we choose a superposition of two Yukawa interactions of Malfliet-Tjon type [25]

$$V(\mathbf{p}', \mathbf{p}) = \frac{1}{2\pi^2} \left(\frac{V_R}{(\mathbf{p}' - \mathbf{p})^2 + \mu_R^2} - \frac{V_A}{(\mathbf{p}' - \mathbf{p})^2 + \mu_A^2} \right). \quad (5.1)$$

The parameters are given in Table VII, and fitted such that the potential supports a two-body bound state, the ‘deuteron’, at -2.23 MeV. As first result we show in Fig. 3 the total cross section together with the total elastic and total break-up cross section as function of the laboratory projectile energy. In addition, the total cross section is also evaluated via the optical theorem as a test of our numerics. This duplicates the information already given in Table III. We see that the optical theorem is quite well fulfilled. The figure shows that at roughly 1 GeV the total elastic and total break-up cross section become equal in magnitude in our model.

Next we show in Fig. 4 the angular distribution in elastic scattering for a set of selected energies. In addition to the exact Faddeev result, the cross sections are evaluated in first order in the two-body t -matrix, second order in t , third order in t , and 4th order in t , and displayed. First we notice that with increasing energy the cross section in forward direction decreases. Furthermore, for all energies shown, the first rescattering (2nd order in t) always increases the cross section, and subsequent rescatterings lower it again. As expected, for the lowest energy, 0.2 GeV, rescattering terms of higher order are important, and even the 4th order is not yet close to the full result. The same is true for 0.8 GeV. We notice, that even at 1 GeV two rescattering terms (3rd order in t) are necessary to come into the vicinity of the final result. The same is true for 0.5 GeV.

In view of the standard ‘ t - ρ ’ impulse approximation for the optical potential in nucleon-nucleus scattering employed at intermediate energies[26], it is interesting to notice that the first order result in t in our model study is quite insufficient. Even at energies larger than 0.5 GeV rescattering corrections up to the 3rd order are required to come close to the exact result for small scattering angles. Therefore it seems to be likely that the first order impulse approximation in nucleon-nucleus scattering is insufficient.

In case of inelastic processes we first regard the semi-exclusive reaction $d(N, N')$ where only one nucleon is detected. We choose three different laboratory energies, 200 MeV, 500 MeV, and 1 GeV and show the inclusive cross section as a few selected angles for the detected nucleon. The results are shown in Figs. 5 through 9.

At 0.2 GeV the semi-exclusive cross section is given in Fig. 5 for the emission angle 24° and in Fig. 6 for the emission angle 39° . Both figures show in the upper panel the entire energy range of the emitted particle. Since the cross section varies by two orders of magnitude, we display it in a logarithmic scale. In order to better flash out the peak structures, the two lower panels show the high and low energies of the emitted particle in a linear scale. Together with the full solution of the Faddeev equation (solid line) we display the sums of the lowest orders of the multiple scattering series as indicated in the figure. The peak at the highest energy of the emitted particle is the socalled final state interaction (FSI) peak, which only develops when rescattering terms are taken into account. This peak is a general feature of

semi-exclusive scattering and is present for all energies. The next peak is the quasi-free (QFS) peak, and one sees that at both angles one needs at least rescattering of 4th order to come close to the full result. However, in contrast to the smaller angle, at the larger angle, 39° in Fig. 6, the first order result for the larger energies is surprisingly close to the full solution, though the multiple scattering series is by no means converged, as the following higher orders indicate. We also observe that the QFS peak moves to lower energies of the emitted particle with increasing emission angle. At both angles the very low energies of the emitted particle exhibit a strong peak in first order, which is considerably lowered by the first rescattering. Here the calculation up to 3rd order in the multiple scattering series seems already sufficient.

For 0.5 GeV incident energy the semi-exclusive cross section is given in Fig. 7 for the emission angle 24° and in Fig. 8 for the emission angle 36° . We again see three peaks along the energy axis of the detected nucleon, the FSI and QFS peaks as well as the peak at the extreme low energy of the emitted particle. Again we see that the results based on first and second order in t alone are quite insufficient and higher order rescatterings can not be neglected. It is also interesting to observe that at 24° , Fig. 7, the third and higher order rescattering terms shift the peak to higher energies, whereas at the larger angle of 36° the peak positions of the various orders coincide more or less and agree with the peak position of the full calculation. Again, for the peak for the very low energies of the emitted particle, the 3rd order calculation agrees already quite well with the full result.

At 1 GeV the situation is similar. As examples we have selected two angles, 18° displayed in Fig. 9 and 30° displayed in Fig. 10. For the small emission angle the second rescattering shifts the QFS peak towards higher energies, at the larger angle this is not the case. It seems that at the larger angle (Fig. 10) the multiple scattering series converges a little faster with respect to the higher orders compared to the smaller angle (Fig. 9). The final result for the peak at the very low energy of the emitted particle is as before reached with two rescattering contributions. It is remarkable that for the energies between about 200 and 500 MeV of the emitted particle the first rescattering contributes almost an order of magnitude to the cross section.

We can make a first contact to calculations based on realistic nucleon-nucleon (NN) forces. In Ref. [17] the semi-exclusive process $d(p, n)$ has been determined in first order in t based on the NN potentials AV18 [27] and Bonn-B [28]. In the upper panel of Fig. 11 we compare our first order calculation at projectile laboratory energy 495 MeV and 18° emission angle with the first order calculations from Ref. [17] based on the two realistic potentials. The position of the peak is only determined through kinematics, thus the peak position coincides for all three calculations. Though our model calculation refers to bosons and the potential contains only the crude features of a central short range repulsion and intermediate range attraction, the magnitudes of the cross sections differ only by roughly 10%. In the lower panel we show the contributions of the first orders of the multiple scattering series successively summed together with the exact solution of the Faddeev equation for our model. At this angle and energy the contribution of the first rescattering (2nd-order in the multiple scattering series) is quite weak, the contributions of the next two orders are large and lower the size of the peak. At the very high energies of the emitted particle, the 4th order in the multiple scattering series is still not yet close to the exact result. Therefore we conjecture that at this energy calculations with realistic forces will also require higher order rescattering contributions.

Finally we comment on a recently measured and analyzed reaction $pd \rightarrow (pp)n$ at high momentum transfer [29, 30]. In this experiment the break-up configuration has been chosen such that the neutron is ejected at extreme backward angles, and the two protons at extreme forward angles. The measurement was carried out at GeV laboratory energies. The experimental data [29] have been analyzed in Ref. [30] using first and second order processes in the NN t -matrix including a Δ -isobar mechanism. Within our nonrelativistic toy model for three bosons we are of course unable to analyze the data. However, within our model we can give a clear answer whether higher order rescattering processes are essential in this reaction. In [29, 30] the data are integrated over a small interval of the relative pp energy between 0 and 3 MeV, and averaged over the neutron c.m. angle in the interval between 172° and 180° . In our qualitative study we fix the c.m. angle of one particle at 180° , but integrate over the relative energy $E_{pp} = p^2/m$ of the two other particles between 0 and 3 MeV. Thus, we evaluate the cross section

$$\frac{d\sigma}{d\Omega_q} = (2\pi)^4 \left(\frac{2}{3}\right)^2 \frac{m^2}{q_0} \int_0^{\sqrt{mE_{pp}}} dp p^2 q \int d\hat{p} |U_0(p, x_p, x_{pq}^{q_0}, x_q = -1, q, q_0)|^2. \quad (5.2)$$

Since we choose the z-axis parallel to $\hat{\mathbf{q}}_0$, and $\hat{\mathbf{q}}$ is antiparallel to $\hat{\mathbf{q}}_0$, the φ_p dependence is directly given by $x_{pq}^{q_0} = \cos \varphi_p$. Our calculations are carried out for projectile laboratory energies between 0.2 and 1 GeV, and are displayed in Fig. 12. Here we compare different low orders in the two-body t -matrix with the full solution of the Faddeev equation. We notice that all our calculations exhibit a smooth fall-off as function of the projectile energy. This behavior is present in the data of Ref. [29]. None of our calculations shows a dip structure around 0.7 GeV as indicated for some of the calculations in Ref. [30]. The reason may be that our calculation is carried out in three dimension, i.e. all partial waves are included exactly, whereas in Ref. [30] only the lowest partial waves are considered. At low projectile energies rescattering terms of higher order still give considerable contributions to the cross section. At 1 GeV the first order

calculation is an order of magnitude smaller than the result of the full calculation. It is interesting to notice that at 1 GeV the contribution from the first rescattering is relatively small, and one needs to go to the 3rd order in t to come close to the full result for this particular break-up configuration.

In addition to the specific break-up configuration described above, a measurement of the extreme backward scattering elastic pd cross section has been investigated in [30]. Instead of a forward scattered pp pair with very small relative energy, one now has a forward going deuteron. This situation corresponds to elastic scattering from a deuteron at backward angle. To investigate the influence of rescattering for this reaction we plot in Fig. 13 the backward angle of the elastic cross section at energies from 0.2 to 1 GeV, and compare the result of the full Faddeev calculation with calculations based on low orders in the multiple scattering series. The figure shows that the first order calculation is insufficient over the entire energy regime considered, except of course for the crossing point around 0.5 GeV. The first rescattering contribution (2nd order calculation), though close at 0.2 GeV, is insufficient below roughly 0.9 GeV. The figure also shows that at about 0.9 GeV the relative magnitude of contributions from the second and higher rescattering become small. Thus, we conclude that at 1 GeV one needs at least one rescattering to be in the vicinity of the full result for the elastic cross section at the backward angle.

VI. SUMMARY AND CONCLUSIONS

In this study we perform fully converged Faddeev calculations for three identical bosons interacting by non-separable forces in the intermediate energy range between about 0.2 and 1.0 GeV. To the best of our knowledge these are the first calculations of this kind. The key point is to neglect the partial wave decomposition generally used at low energies and to work directly with momentum vectors. Thus all partial waves are exactly included. Important is the suitable choice of variables. Besides the two magnitudes of the two relative Jacobi momenta \mathbf{p} and \mathbf{q} we choose the angles between the vectors \mathbf{p} and \mathbf{q}_0 and between \mathbf{q} and \mathbf{q}_0 , where \mathbf{q}_0 is the projectile momentum. The fifth variable is the angle between the two planes spanned by \mathbf{p} , \mathbf{q}_0 and \mathbf{q} , \mathbf{q}_0 . In the technical piece of the work we introduce for the first time a spline based integration of the moving logarithmic singularities, which is a very valuable alternative to procedures used so far. The numerical results are well converged as documented in Section III. In Section V we show elastic and inelastic (break-up) cross sections in the above mentioned intermediate energy range. We focus on the question how many orders of rescattering beyond the often used first order calculation in the two-body t -matrix are needed to come close to the full Faddeev result. We find that in nearly all cases studied processes of at least 2nd and 3rd order rescattering are required. Whether this will be also required in performing calculations with realistic dynamical inputs has to be seen in the future.

In one case we can make first contact to a result based on the NN forces AV18 and Bonn B, which are considered to be realistic in the sense that they describe all NN data below 350 MeV extremely well. This was the semi-exclusive cross section at 495 MeV evaluated in first order in the NN t -matrix. Of course, at that energy AV18 and Bonn-B are at the upper limit of their applicability. Despite our simple two-body model force, a superposition of two Yukawa interactions, one attractive the other repulsive, our results turns out to be within about 10% to the calculation based on the realistic models. This shows that our investigations might allow some conclusions about results based on present and future models with more dynamical inputs.

As a first example for considering data in the light of our toy model we study the extreme backward elastic dN scattering over the energy range from 0.2 to 1.0 GeV. We find that first order results in the two-body t -matrix are totally insufficient and only around 1 GeV the first order rescattering comes close to the full result. Parallel to those data in elastic scattering in [29, 30] the complete break up process $d(p,n)pp$ has also been investigated. Here the neutron was ejected antiparallel to the beam direction and the two protons at extreme forward angles with a very small relative energy. Again we study the significance of rescattering processes, and find that for this particular break-up configuration two rescatterings are necessary to get close to the result of the full Faddeev calculation.

In conclusion we can say that the three-body Faddeev equations can be safely solved at intermediate energies using directly momentum vectors. Calculations based on partial wave decomposition would be hardly feasible at these energies.

Further studies scanning the complete three-body phase space for the total break-up are underway. This may be important in order to shed light on previous theoretical analysis of $p(d,ppn)$ reactions which relied on low order reaction mechanisms.

Based on our current experience it appears that if low order rescattering processes will turn out to be sufficient for certain phase space regions, realistic calculations including spin and isospin will be feasible, even including three-body forces. A first step evaluating the $d(p,n)pp$ break-up cross section in first order with a currently used two-pion exchange three-nucleon force model is already under way [31]. What is badly needed now are realistic models for nuclear forces in the intermediate energy regime we study. This paper allows us to conclude that it will be feasible to extend the calculations to realistic dynamics.

Acknowledgments

This work was performed in part under the auspices of the U. S. Department of Energy under contract No. DE-FG02-93ER407561 with Ohio University. We thank the National Energy Research Supercomputer Center (NERSC) for the use of their facilities. We thank I. Fachruddin for allowing us to use his results for comparison with ours. One of us (W.G.) would like to thank K. Miyagawa for fruitful collaboration on the spline based integration of the logarithmic singularities.

APPENDIX A: THE φ'' INTEGRATION

According to Eqs. (2.19), (2.18), and (2.20) the φ'' -integration for fixed p , q , x_p , x_q , $x_{pq}^{q_0}$, q'' , and x'' can be written as

$$I(\varphi_{q_0}, \varphi_p) = \int_0^{2\pi} F[\cos(\varphi'' - \varphi_{q_0})]G[\cos(\varphi'' - \varphi_p)]d\varphi''. \quad (\text{A1})$$

where the F and G are known functions from \hat{t}_s and \hat{T} . The substitution $\varphi' = \varphi'' - \varphi_{q_0}$ leads to

$$\begin{aligned} I(\varphi_{q_0}, \varphi_p) &= \int_0^{2\pi} F[\cos \varphi']G[\cos(\varphi' - (\varphi_p - \varphi_{q_0}))]d\varphi' \\ &\equiv I(\varphi_{q_0} - \varphi_p). \end{aligned} \quad (\text{A2})$$

Moreover, splitting this integral as

$$\begin{aligned} I(\varphi_{q_0} - \varphi_p) &= \int_0^\pi F[\cos \varphi']G[\cos(\varphi' - (\varphi_p - \varphi_{q_0}))]d\varphi' \\ &+ \int_\pi^{2\pi} F[\cos \varphi']G[\cos(\varphi' - (\varphi_p - \varphi_{q_0}))]d\varphi' \end{aligned} \quad (\text{A3})$$

and substituting $\varphi' = 2\pi - \varphi''$ in the second integral, one obtains

$$I(\varphi_p - \varphi_{q_0}) = \int_0^\pi F[\cos \varphi''] \left(G[\cos(\varphi'' - (\varphi_p - \varphi_{q_0}))] + G[\cos(\varphi'' + (\varphi_p - \varphi_{q_0}))] \right) d\varphi'' \equiv I(|\varphi_p - \varphi_{q_0}|). \quad (\text{A4})$$

Consequently, the result for the φ -integration in Eq. (A2) or Eq. (A4) does not depend on the choice of the sign in $\sin(\varphi_p - \varphi_{q_0}) = \pm\sqrt{1 - \cos^2(\varphi_p - \varphi_{q_0})}$. Only $\cos(\varphi_p - \varphi_{q_0})$ is fixed by Eq. (2.21), and has to be known.

Since the integral I in Eq. (A4) depends only on the difference of the angles $(\varphi_p - \varphi_{q_0})$, one can choose φ_{q_0} arbitrarily, and thus $\sin \varphi_{q_0}$ and $\cos \varphi_{q_0}$ required in Eq. (2.18). Moreover, the trivial identities

$$\begin{aligned} \cos \varphi_p &= \cos \varphi_{q_0} \cos(\varphi_p - \varphi_{q_0}) - \sin \varphi_{q_0} \sin(\varphi_p - \varphi_{q_0}), \\ \sin \varphi_p &= \sin \varphi_{q_0} \cos(\varphi_p - \varphi_{q_0}) + \cos \varphi_{q_0} \sin(\varphi_p - \varphi_{q_0}). \end{aligned} \quad (\text{A5})$$

are the input for $\cos(\varphi_p - \varphi'')$ needed in Eq. (2.20). The arbitrary choice of φ_{q_0} is a good check for the numerical correctness of the choice of variables, and we carried out those tests.

- [1] J.L. Friar, G.L. Payne, W. Glöckle, D. Hüber, H. Witala, Phys. Rev. C **51**, 2356 (1995).
- [2] H. Witala, Th. Cornelius, W. Glöckle, Few-Body Systems **3**, 123 (1988).
- [3] A. Kievsky, M. Viviani, and S. Rosati, Phys. Rev. C **64**, 024002 (2001).
- [4] M. Viviani, A. Kievsky, and S. Rosati, Few-Body Systems **30**, 39 (2001).
- [5] W. Glöckle, et. al., Phys. Rep. **274**, 107 (1996).
- [6] W. Glöckle in ‘Scattering, Scattering and Inverse Scattering in Pure and Applied Science’, Eds. R. Pike and P. Sabatier, Academic Press, p. 1339-1359 (2002).
- [7] J. Kuros-Zolmericzuk, et. al., Phys. Rev. C **66**, 024004 (2002).
- [8] H. Witala, et. al., Phys. Rev. C **63**, 024007 (2001).
- [9] K. Chmielewski, A. Deltuva, A.C. Fonseca, S. Nemoto, P.U. Sauer, Phys. Rev. C **67**, 014002 (2003).
- [10] A. Arriaga, V. R. Pandharipande, and R. B. Wiringa, Phys. Rev. C **52**, 2362 (1995).
- [11] J. Carlson, Phys. Rev. C **36**, 2026 (1987).
- [12] J. Carlson, Phys. Rev. C **38**, 1879 (1988).
- [13] J. G. Zabolitzki, K. E. Schmidt, and M. H. Kalos, Phys. Rev. C **25**, 1111 (1982).
- [14] J. Carlson and R. Schiavilla, Rev. Mod. Phys. **70**, 743 (1998).
- [15] Ch. Elster, W. Schadow, A. Nogga and W. Glöckle, Few-Body System **27**, 83 (1999).
- [16] H. Liu, Ch. Elster and W. Glöckle, Few-Body System **33**, 241 (2003).
- [17] I. Fachruddin, Ch. Elster, W. Glöckle, Phys. Rev. C **68**, 054003 (2003).
- [18] W. Glöckle, *The Quantum Mechanical Few-Body Problem* (Springer-Verlag, Berlin-Heidelberg, 1983).
- [19] W. Schadow, Ch. Elster, W. Glöckle, Few-Body Systems **28**, 15 (2000).

- [20] Ch. Elster, J. H. Thomas and W. Glöckle, Few-Body System **24**, 55 (1998).
- [21] G. A. Baker and J. L. Gammel, ed., *The Padé Approximation in Theoretical Physics* (Academic Press, New York, 1970).
- [22] D. Hüber, Ph.D. thesis, Bochum University, Bochum, Germany, 1996.
- [23] D. Hüber, H. Witala, A. Nogga, W. Glöckle and H. Kamada, Few-Body System, **22**, 107 (1997).
- [24] H. Liu, PhD thesis, Ohio University, in preparation.
- [25] R.A. Malfliet, A.J. Tjon, Nucl. Phys. A, **127**, 161 (1969).
- [26] L. Ray, G.W. Hoffmann, Phys. Rev. C**31**, 538 (1985); R. Crespo, R.C. Johnson, J.A. Tostevin, Phys. Rev. C**44**, R1735 (1991); Ch. Elster, T. Cheon, E.F. Redish, P.C. Tandy, Phys. Rev. C**41**, 814 (1990).
- [27] R. B. Wiringa, V. G. J. Stoks, R. Schiavilla, Phys. Rev. C**51**, 38 (1995).
- [28] R. Machleidt, Adv. Nucl. Phys. **19**, 189 (1989).
- [29] V. Komarov *et al.*, Phys. Lett. B **553**, 179 (2003).
- [30] J. Haidenbauer, Y.N. Uzikov, Phys. Lett. B **562**, 227 (2003).
- [31] I. Fachruddin, private communication.

$E_{lab}[GeV]$	p	x_p	$x_{pq}^{q_0}$	x_q	q, q''	x''	φ''	$\theta_{cm}[\text{deg}]$	$\frac{d\sigma_{el}}{d\Omega} [\text{mb}]$	p	x_p	$x_{pq}^{q_0}$	x_q	q, q''	x''	φ''	$\theta_{cm}[\text{deg}]$	$\frac{d\sigma_{el}}{d\Omega} [\text{mb}]$
0.01	49	4	4	49	4	4		0.0	498.57	49	12	12	12	49	12	12	0.0	539.24
								46.4	177.68								46.4	182.08
								90.1	51.01								90.1	40.16
								135.8	144.96								135.8	179.09
								180.0	834.18								180.0	764.95
0.01	49	8	8	8	49	8	8	0.0	556.69	49	16	16	16	49	16	16	0.0	537.53
								46.4	173.82								46.4	179.59
								90.1	69.05								90.1	46.27
								135.8	165.08								135.8	183.49
								180.0	631.95								180.0	766.87
0.5	49	12	12	12	49	12	12	0.0	529.26	49	20	20	20	49	20	20	0.0	515.98
								21.8	2.1713								21.8	15.019
								62.1	0.0453								62.1	0.0856
								93.4	0.0031								93.4	0.0045
								151.5	0.0037								151.5	0.0040
0.5	49	16	16	16	16	16	16	0.0	487.02	49	24	20	20	49	20	20	0.0	517.33
								21.8	9.0338								21.8	15.301
								62.1	0.0776								62.1	0.0858
								93.4	0.0039								93.4	0.0045
								151.5	0.0031								151.5	0.0040
0.5	49	20	20	16	49	16	20	0.0	509.09	49	20	20	24	49	24	20	0.0	519.42
								21.8	10.128								21.8	16.374
								62.1	0.0806								62.1	0.0888
								93.4	0.0041								93.4	0.0046
								151.5	0.0032								151.5	0.0044
0.5	49	20	16	20	49	20	16	0.0	516.43	49	23	23	24	49	24	20	0.0	519.39
								21.8	14.628								21.8	16.209
								62.1	0.0798								62.1	0.0883
								93.4	0.0041								93.4	0.0045
								151.5	0.0047								151.5	0.0041

TABLE I: The elastic differential cross section at selected angles calculated from a Malfliet-Tjon type potential at two selected energies (0.01 and 0.5 GeV) as function of the grid points on which \hat{T} is defined in Eq. (2.19). The double prime quantities represent the integration variables.

$E_{lab}[GeV]$	p	x_p	$x_{pq}^{q_0}$	x_q	q, q''	x''	φ''	σ_{opt} [mb]	σ_{el} [mb]	σ_{br} [mb]
0.01	49	4	4	4	49	4	4	1913.48	1799.08	67.81
	49	8	8	8	49	8	8	1886.84	1807.50	70.14
	49	12	12	12	49	12	12	1904.99	1820.77	73.75
	49	16	16	16	49	16	16	1903.22	1820.46	73.20
0.5	49	12	12	12	49	12	12	92.41	51.35	81.99
	49	16	16	16	49	16	16	100.67	53.71	38.79
	49	20	20	16	49	16	20	100.76	55.77	38.62
	49	20	16	20	49	20	16	107.85	63.11	37.50
	49	20	20	20	49	20	20	107.25	63.40	37.89
	49	24	20	20	49	20	20	107.71	63.32	37.88
	49	20	20	24	49	24	20	108.50	63.84	38.40
	49	23	23	24	49	24	20	108.69	63.22	38.09

TABLE II: The total elastic and break-up cross sections together with the total cross section extracted via the optical theorem calculated from a Malfliet-Tjon type potential at two selected energies (0.01 and 0.5 GeV) as function of the grid points. The double prime quantities are the integration variables.

E_{lab} [GeV]	$\sigma_{el}^{q_0}$ [mb]	σ_{el}^q [mb]	$\sigma_{br}^{q_0}$ [mb]	σ_{br}^q [mb]	σ_{br}^p [mb]	$\sigma_{opt}^{q_0}$ [mb]	σ_{opt}^q [mb]
0.003	2561.74	2561.14	0.0	0.0	0.0	2562.65	2562.65
0.01	1820.71	1820.51	73.69	73.55	73.13	1902.63	1902.56
0.2	204.30	204.30	53.92	53.93	53.93	245.57	245.57
0.5	63.22	63.23	38.09	38.11	38.17	108.69	108.69
0.8	30.73	30.74	27.59	27.60	27.63	66.70	66.70
1.0	21.90	21.90	23.44	23.46	23.40	49.59	49.59

TABLE III: The total elastic cross section, total breakup cross section and total cross section extracted via the optical theorem calculated in different coordinate systems at selected energies. The choice of coordinate system, i.e. which vector is aligned parallel to the z-axis, is indicated by the superscripts q_0 , q and p .

E_{lab} [GeV]	θ_{cm} [deg]	$\frac{d\sigma^{el}}{d\Omega_{cm}} _T$ [mb]	$\frac{d\sigma^{el}}{d\Omega_{cm}} _{T'}$ [mb]
0.01	0.0	537.536	537.536
	21.8	420.036	420.036
	62.1	70.726	70.725
	93.4	38.289	38.289
	151.5	227.899	227.899
0.2	0.0	676.821	676.821
	21.8	148.880	148.880
	62.1	0.363	0.363
	93.4	0.223	0.223
	151.5	0.010	0.010
0.5	0.0	519.389	519.389
	21.8	16.209	16.209
	26.3	4.430	4.430
	62.1	0.088	0.088
	93.4	0.005	0.005
	151.5	0.004	0.004
1.0	0.0	$3.903 \times 10^{+2}$	$3.903 \times 10^{+2}$
	21.8	5.325×10^{-1}	5.325×10^{-1}
	62.1	4.072×10^{-4}	4.072×10^{-4}
	93.4	2.678×10^{-3}	2.678×10^{-3}
	151.5	3.705×10^{-4}	3.703×10^{-4}

TABLE IV: The elastic differential cross sections at different energies for selected scattering angles. The cross section labeled by T results from the converged solution of the integral equation Eq. (2.19). The column labeled T' is calculated by reinserting the original solution into the Faddeev equation with $T' = tP + tG_0PT$. The calculations are based on a Malfliet-Tjon type potential as described in the text.

φ_{q_0} [rad]	$\sigma_{el}^{q_0}$ [mb]	σ_{el}^q [mb]	$\sigma_{opt}^{q_0}$ [mb]	σ_{opt}^q [mb]
0.0	2561.736	2561.138	2562.649	2562.649
$\frac{\pi}{2}$	2560.885	2560.729	2562.496	2562.496
π	2561.550	2561.206	2562.091	2562.091

TABLE V: The total elastic cross sections at $E_{lab} = 3.0$ MeV calculated for different values of the angle φ_{q_0} with the + sign of $\sin(\varphi_p - \varphi_{q_0})$. The calculations are carried out in two different coordinate systems, characterized by the superscripts q_0 and q , which indicate, which vector is chosen to be parallel to the z-axis.

$\text{sign}[\sin(\varphi_p - \varphi_{q_0})]$	$\sigma_{el}^{q_0}$ [mb]	σ_{el}^q [mb]	$\sigma_{opt}^{q_0}$ [mb]	σ_{opt}^q [mb]
+	2561.736	2561.138	2562.649	2562.649
-	2559.674	2559.536	2560.091	2560.091

TABLE VI: The total elastic cross sections at $E_{lab} = 3.0$ MeV calculated for different sign of $\sin(\varphi_p - \varphi_{q_0})$ where $\varphi_{q_0} = 0$. The meaning of the superscripts is the same as in Table V.

V_A [MeV fm]	μ_A [fm^{-1}]	V_R [MeV fm]	μ_R [fm^{-1}]	E_d [MeV]
-626.8932	1.550	1438.7228	3.11	-2.2307

TABLE VII: The parameters and deuteron binding energy for the Malfliet-Tjon type potential of our calculation. As conversion factor We use units such that $\hbar c = 197.3286$ MeV fm = 1.

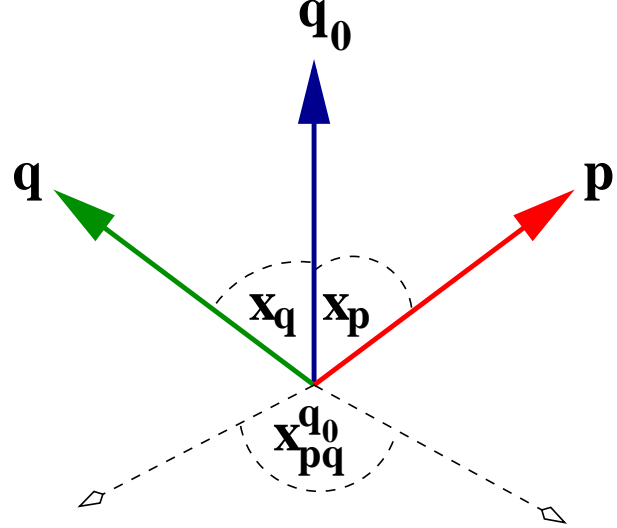


FIG. 1: The geometry of three vectors \mathbf{q}_0 , \mathbf{q} , and \mathbf{p} relevant in the three-body scattering problem. The independent angle variables x_q , x_p , and $x_{pq}^{q_0}$ as defined in Section II are indicated. The dashed arrows represent the normal vectors $(\mathbf{q}_0 \times \mathbf{q})$ and $(\mathbf{p} \times \mathbf{q}_0)$.

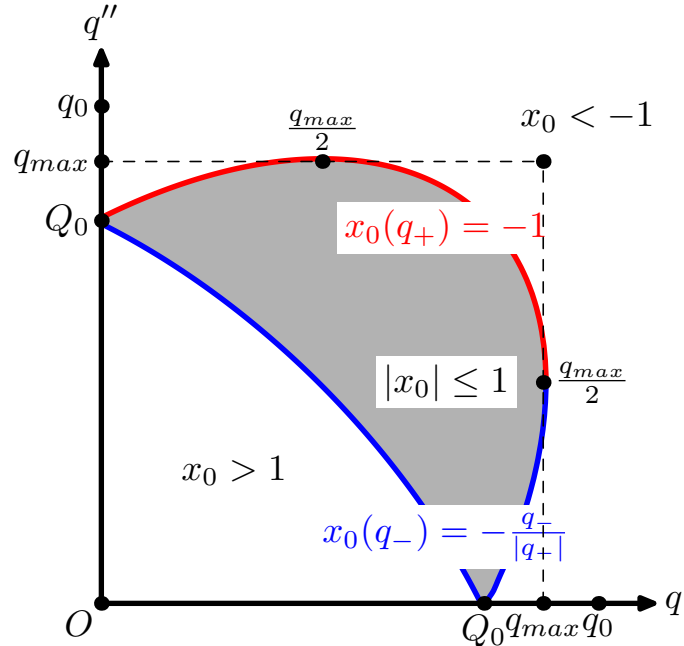


FIG. 2: The region of singularities of the free three-particle propagator as function of the momenta q and q'' . The shaded area in the $q - q''$ plane indicates the region where $|x_0| \leq 1$, i.e. the region where a pole in the x'' -integration occurs. This region is enclosed by the bounding curves q_+ and q_- , which contain the logarithmic singularity as function of q'' as given in Eqs. (4.5) and (4.6).

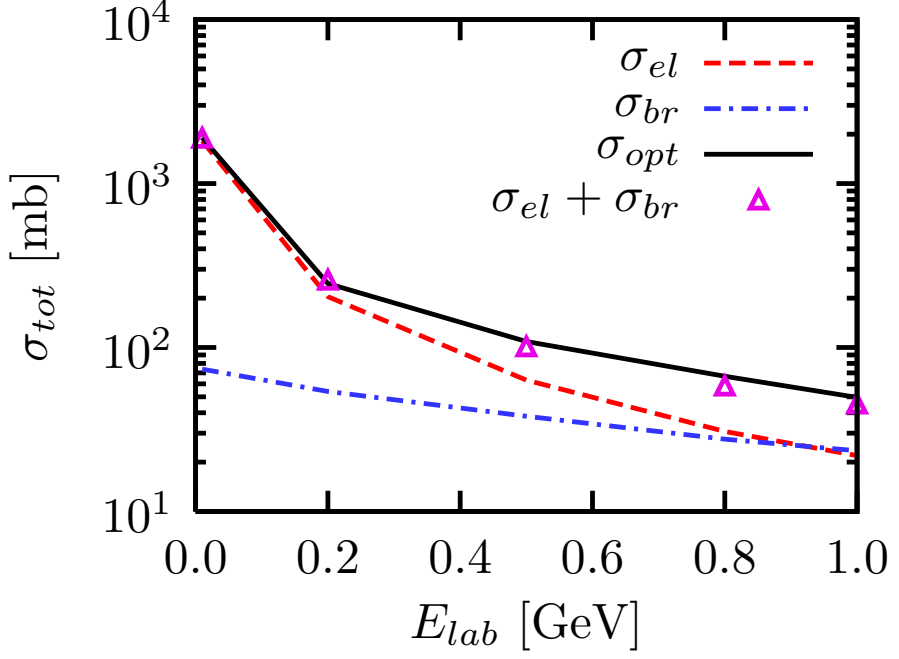


FIG. 3: The total elastic cross section σ_{el} (dashed line), the total break-up cross section σ_{br} (dash-dotted line) and the total cross section evaluated by the optical theorem σ_{opt} (solid line) given as function of the projectile laboratory energy. At selected energies where the calculations have been carried out the sum of the calculated total elastic and break-up cross section, $\sigma_{tot} = \sigma_{el} + \sigma_{br}$, is indicated by the open diamond. The open diamonds coincide with the solid line according to the optical theorem, Eq. 3.23, and the numerical values are given in Table III.

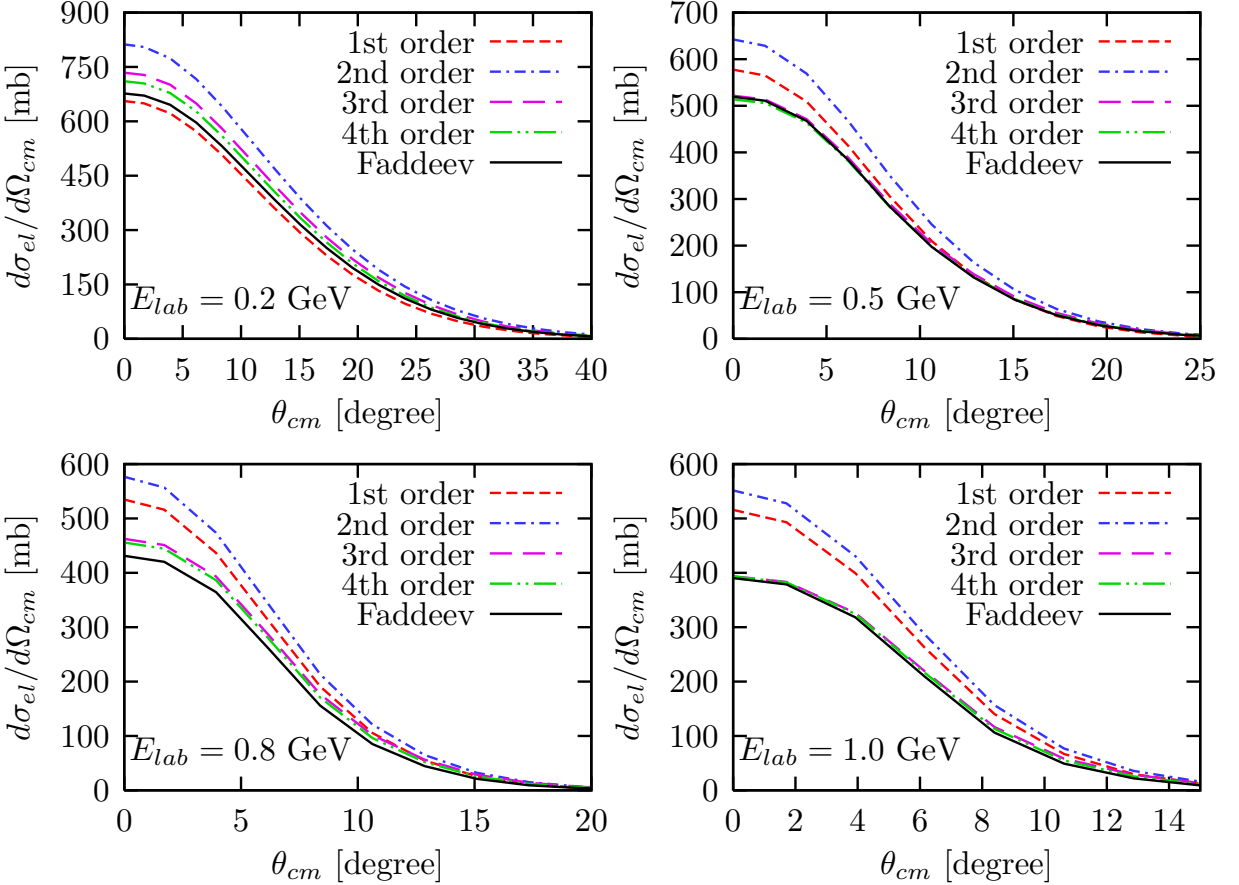


FIG. 4: The elastic differential cross section at 0.2 GeV, 0.5 GeV, 0.8 GeV, and 1.0 GeV projectile energy as function of the laboratory scattering angle. In all cases the solid line represent the full solution of the Faddeev equation. The other lines represent the successive sum of different orders in the multiple scattering series, short-dashed the first order, dash-dot adds up to the 2nd order, long-dashed to the 3rd order, and dash-dot-dot to the 4th order contribution.

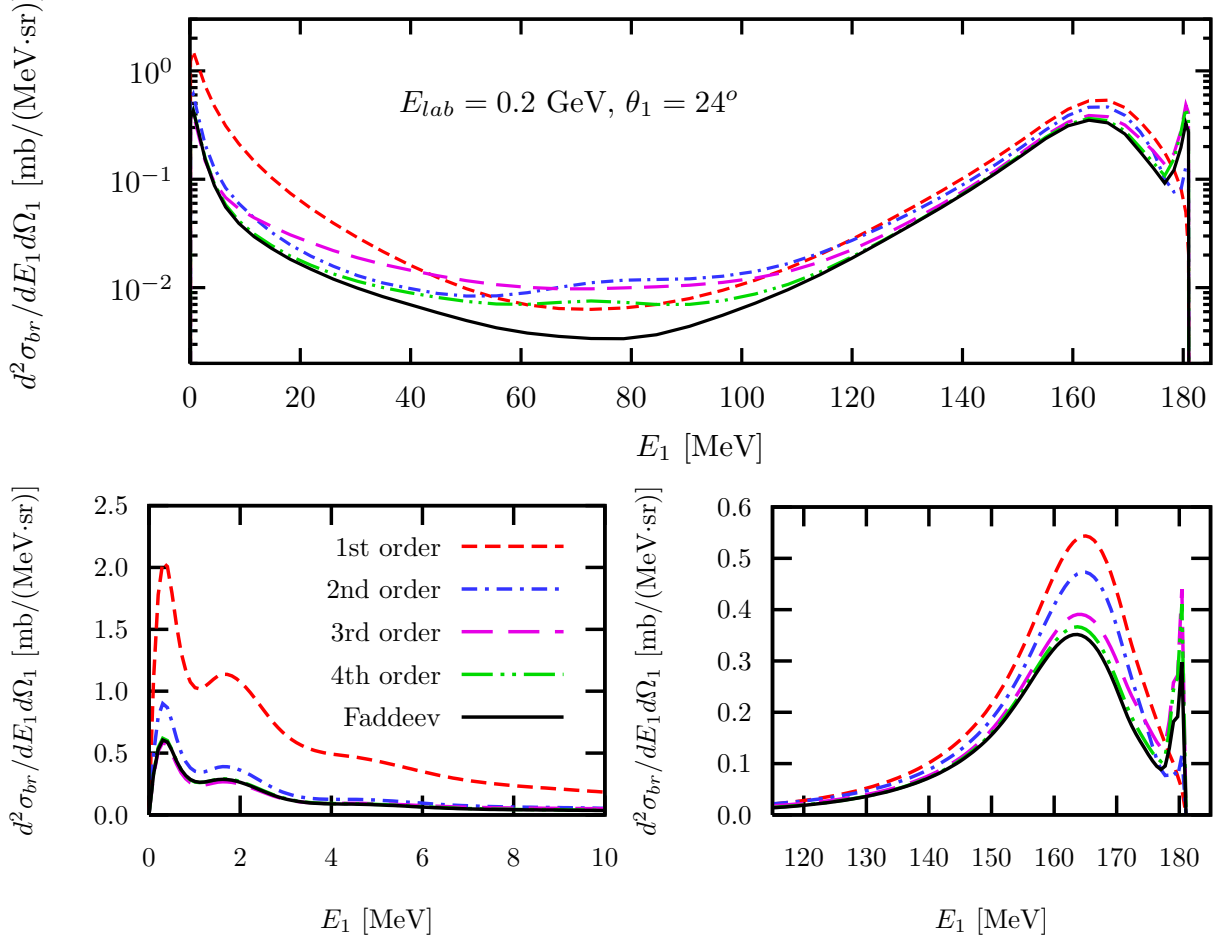


FIG. 5: The semi-exclusive cross section at 0.2 GeV laboratory incident energy and at 24° emission angle of the emitted particle. The upper panel displays the entire energy range of the emitted particle, whereas the two lower panels show only the low and high energies in a linear scale. The full solution of the Faddeev equation is given by the solid line in all panels. The contribution of the lowest orders of the multiple scattering series added up successively is given by the other curves as indicated in the legend of the lower left panel.

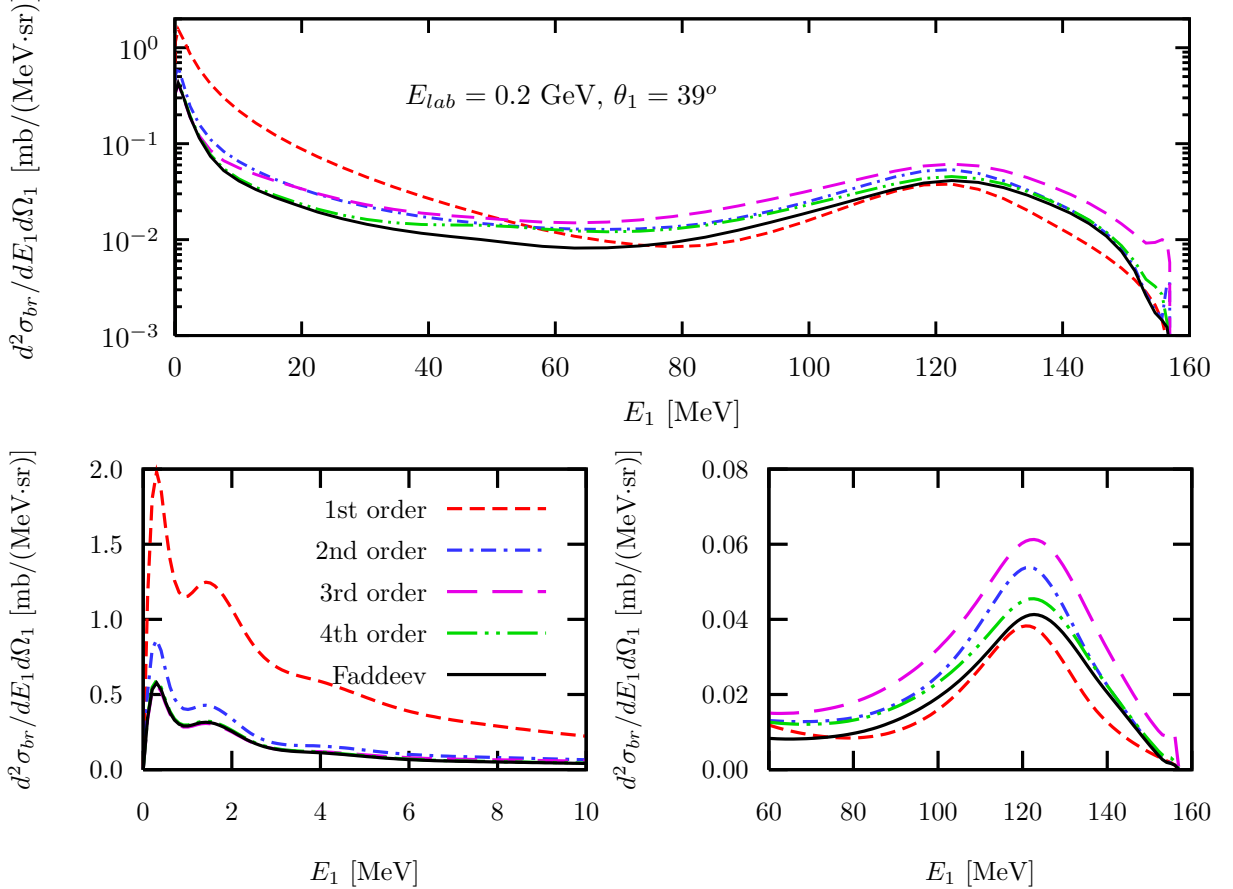


FIG. 6: Same as Fig. 5 but for an angle of 39° of the emitted particle.

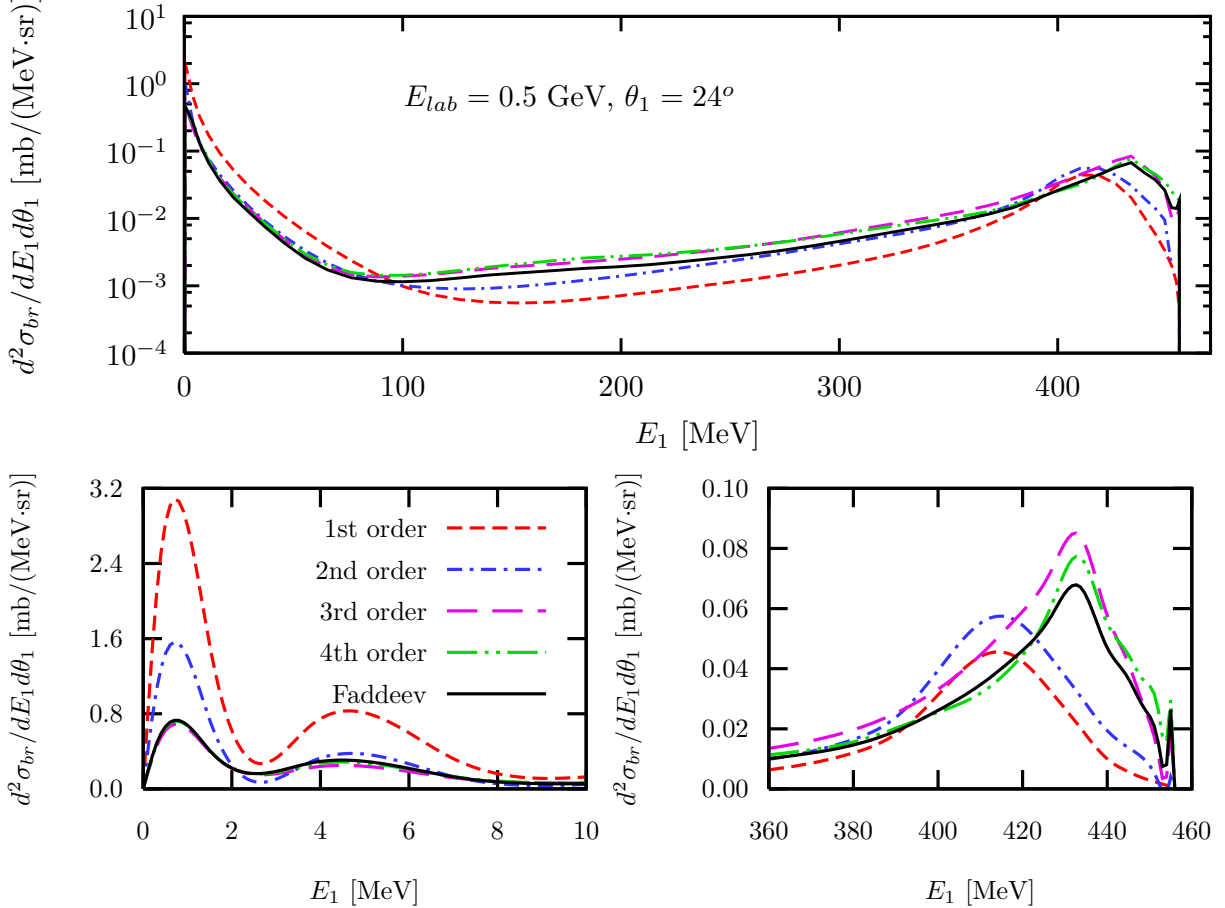


FIG. 7: The semi-exclusive cross section at 0.5 GeV laboratory incident energy and at 24° angle of the emitted particle. The upper panel displays the entire energy range of the emitted particle, whereas the two lower panels show only the low and high energies in a linear scale. The full solution of the Faddeev equation is given by the solid line in all panels. The contribution of the lowest orders of the multiple scattering series added up successively is given by the other curves as indicated in the legend of the lower left panel.

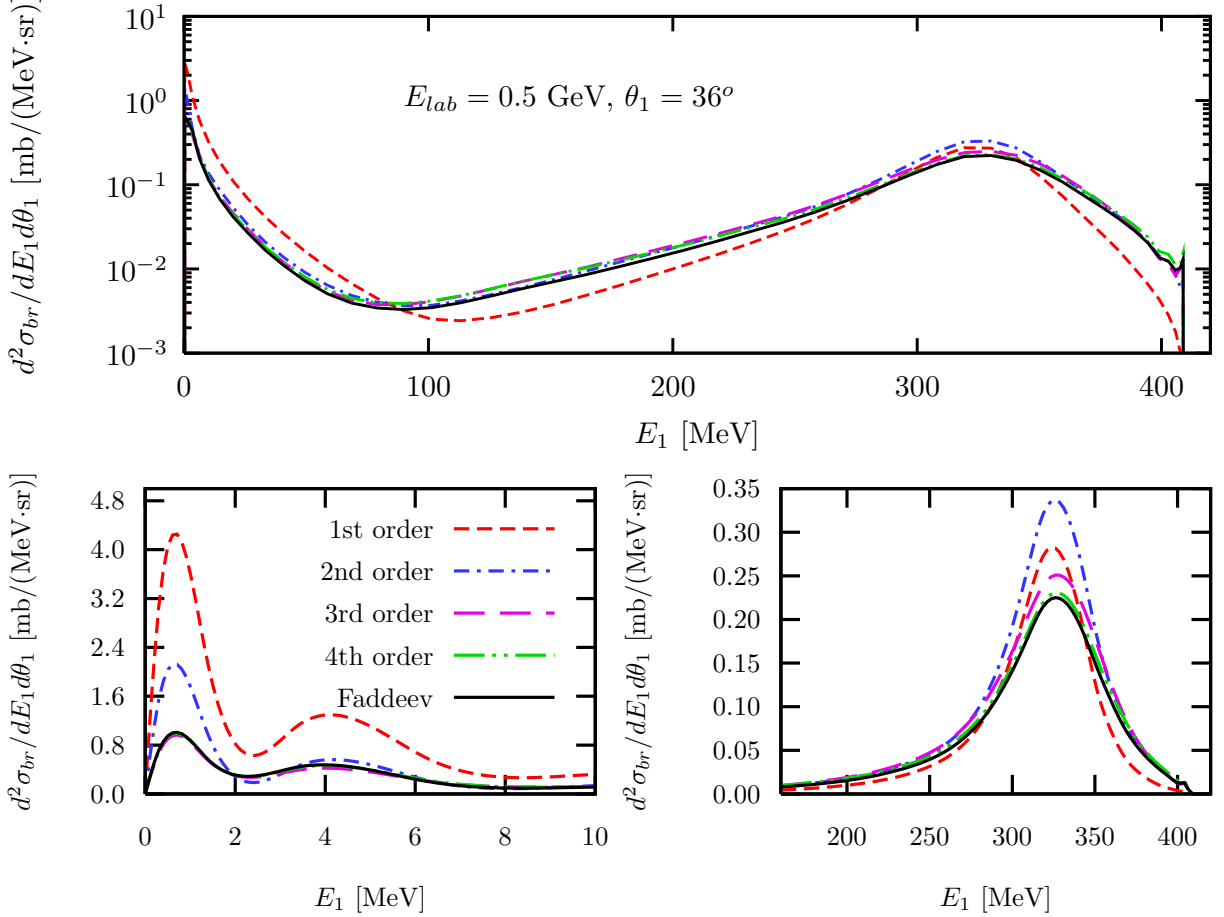


FIG. 8: Same as Fig. 7 but for an angle of 36° of the emitted particle.

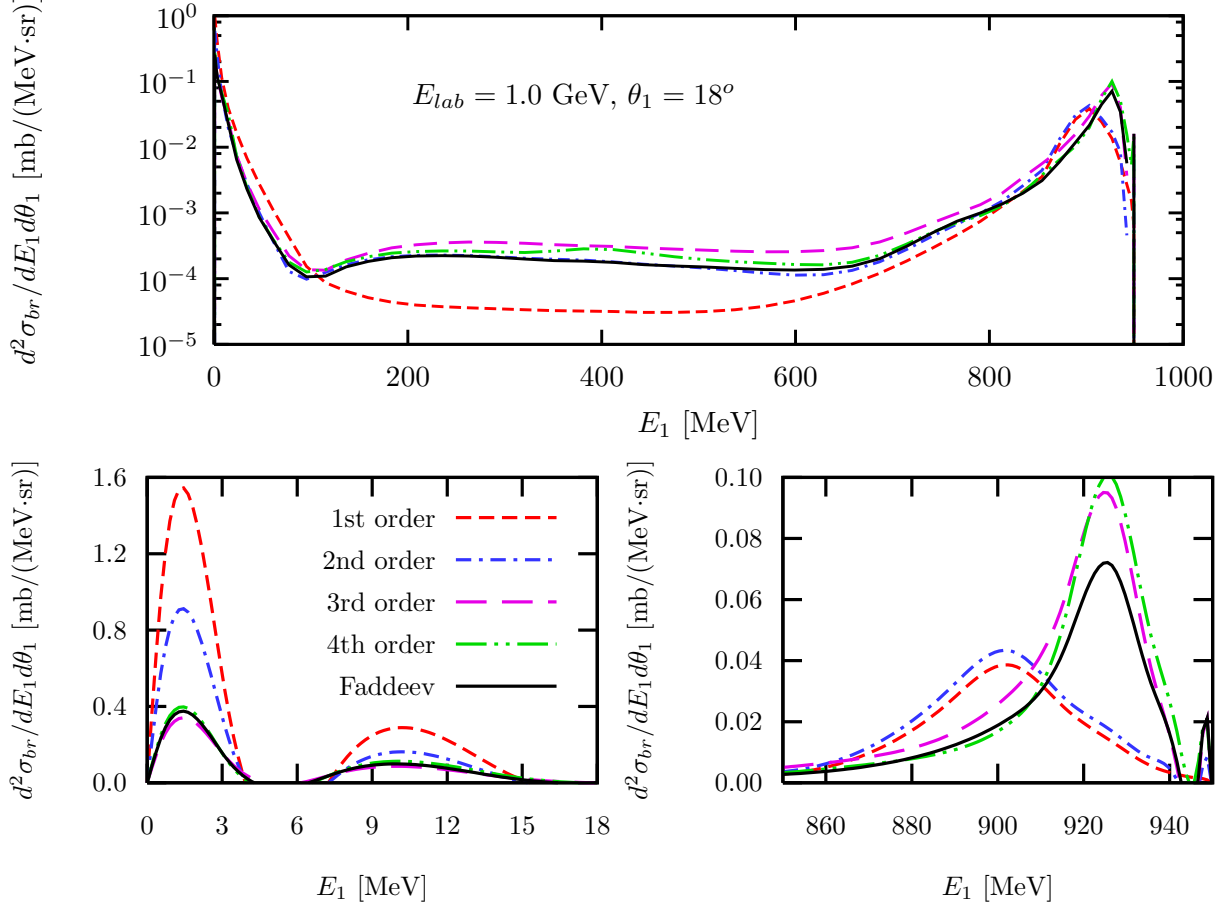


FIG. 9: The semi-exclusive cross section at 1 GeV laboratory incident energy and at 18° angle of the emitted particle. The upper panel displays the entire energy range of the emitted particle, whereas the two lower panels show only the low and high energies in a linear scale. The full solution of the Faddeev equation is given by the solid line in all panels. The contribution of the lowest orders of the multiple scattering series added up successively is given by the other curves as indicated in the legend of the lower left panel.

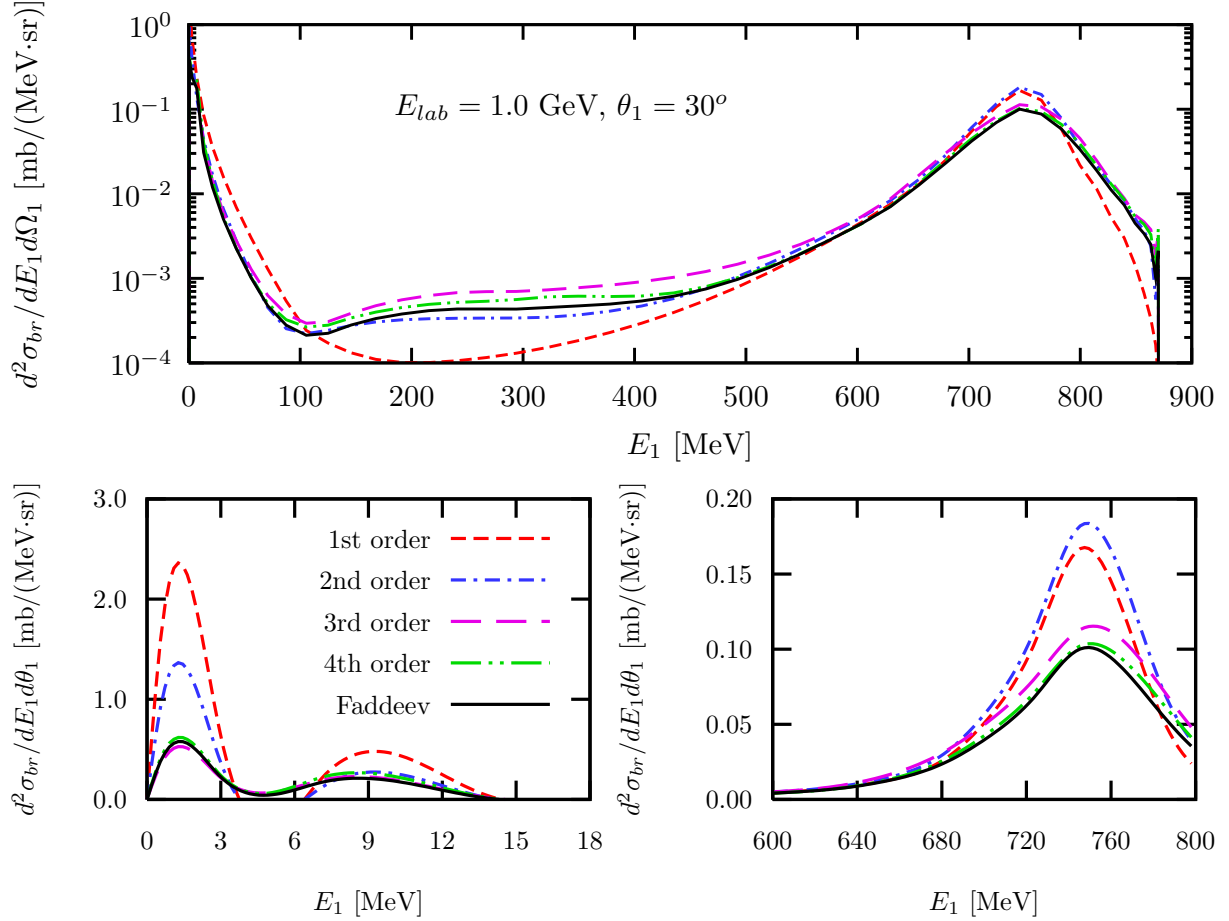


FIG. 10: Same as Fig. 9 but for an angle of 30° of the emitted particle.

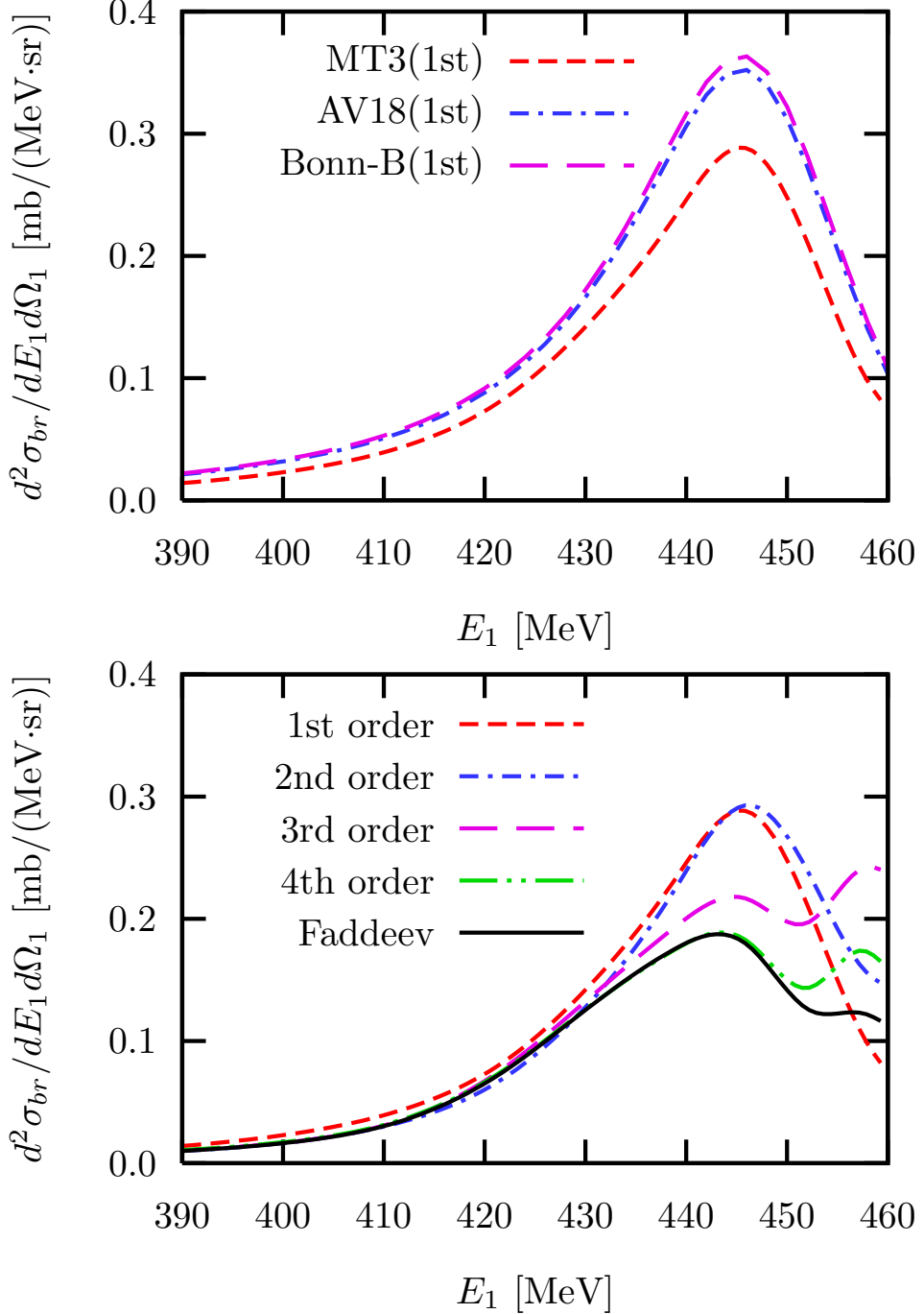


FIG. 11: The semi-exclusive cross section at 495 MeV laboratory incident energy and at 18° angle of the emitted particle. The upper panel displays the first order results obtained from the realistic potentials AV18 [27] (long dashed line) and Bonn-B [28] (dashed-dotted line) together with our calculation based on the scalar MT potential of Eq. 5.2 (dashed line). The lower panel displays again our first order calculation from the upper panel (dashed line), together with a successive addition of the next three rescattering terms. The exact solution of the Faddeev equation is given by the solid line.

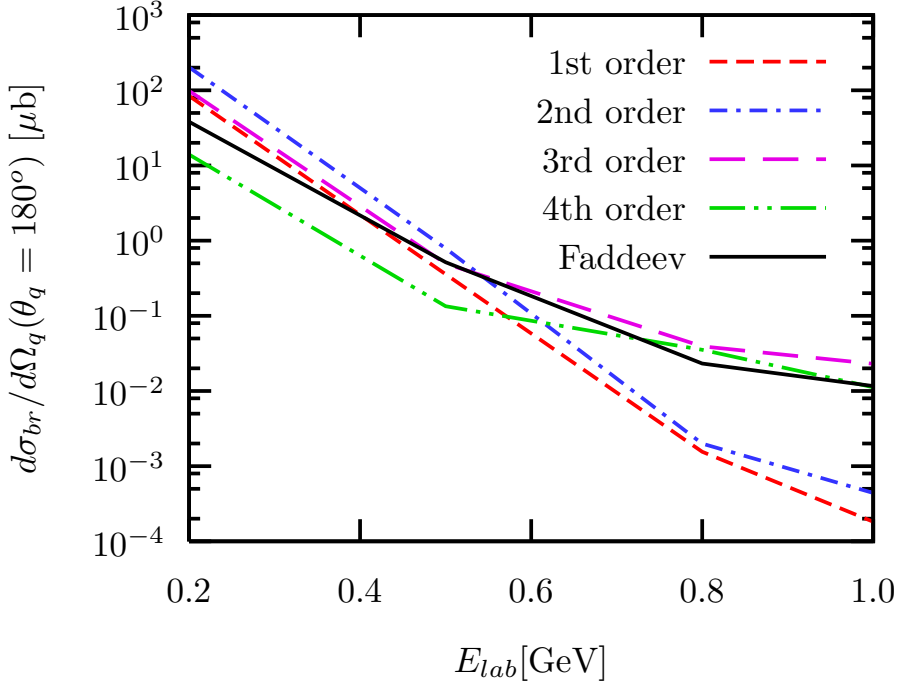


FIG. 12: The cross section (c.m.) for the semi-exclusive break-up reaction in which two particles emerge in forward direction with a relative energy between 0 and 3 MeV, and one particle is detected at backward angle as function of the projectile laboratory energy. The result of the full Faddeev calculation is given by the solid line and is compared with calculations based on the lowest orders of the multiple scattering series in t added up successively as indicated in the legend.

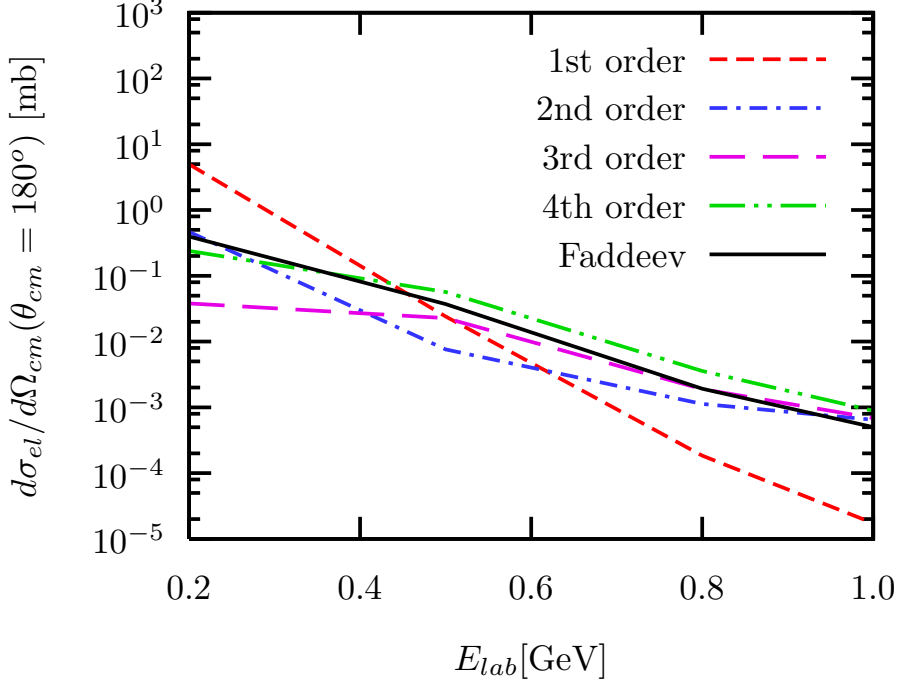


FIG. 13: The elastic cross section (c.m.) at backward angle as function of the projectile laboratory energy. The result of the full Faddeev calculation is given by the solid line and compared with calculations based on the lowest orders of the multiple scattering series in t added up successively as indicated in the legend.